

# LA-UR-12-21067

Approved for public release; distribution is unlimited.

Title: Conceptual Ideas for New Nondestructive UF6 Cylinder Assay Techniques

Author(s): Miller, Karen A.

Intended for: Report



## Disclaimer:

Los Alamos National Laboratory, an affirmative action/equal opportunity employer, is operated by the Los Alamos National Security, LLC for the National Nuclear Security Administration of the U.S. Department of Energy under contract DE-AC52-06NA25396. By approving this article, the publisher recognizes that the U.S. Government retains nonexclusive, royalty-free license to publish or reproduce the published form of this contribution, or to allow others to do so, for U.S. Government purposes. Los Alamos National Laboratory requests that the publisher identify this article as work performed under the auspices of the U.S. Department of Energy. Los Alamos National Laboratory strongly supports academic freedom and a researcher's right to publish; as an institution, however, the Laboratory does not endorse the viewpoint of a publication or guarantee its technical correctness.

**Conceptual Ideas for New Nondestructive  
UF<sub>6</sub> Cylinder Assay Techniques**

*Prepared for:*

*State-of-the-Art NDA Methods Applicable to UF<sub>6</sub> Cylinder Assay: Phase II  
USSP Task A.279*

*International Atomic Energy Agency  
Vienna, Austria*

*Prepared by:*

*Los Alamos National Laboratory  
Pacific Northwest National Laboratory  
Oak Ridge National Laboratory*

*April 2012*

## Table of Contents

I. INTRODUCTION .....	1
II. MONTE CARLO FEASIBILITY STUDY OF AN ACTIVE NEUTRON ASSAY TECHNIQUE FOR UF <sub>6</sub> CYLINDERS USING A CORRELATED INTERROGATION SOURCE .....	3
II.A. Abstract .....	3
II.B. Introduction .....	3
II.C. Monte Carlo Modeling .....	5
II.D. Comparison of Random and Correlated Interrogation Sources .....	6
II.E. Detector Optimization.....	8
II.F. Counting Statistics Projected onto Enrichment .....	10
II.G. Conclusions .....	12
II.H. References .....	13
III. FEASIBILITY ASSESSMENT OF APPLICATION OF NUCLEAR RESONANCE FLUORESCENCE TO ACTIVE UF <sub>6</sub> CYLINDER ENRICHMENT ASSAY .....	14
III.A. Introduction .....	14
III.B. Feasibility Assessment .....	16
III.C. Conclusions .....	20
III.D. References .....	21
IV. MEASUREMENTS OF CONTINUOUS-IN-ENERGY NEUTRON SOURCES USING THE BC-523A CAPTURE-GATED LIQUID SCINTILLATOR.....	22
IV.A. Introduction.....	22
IV.B. Pulse Shape Discrimination for BC-523A .....	22
IV.C. Measurement and Simulation Results for Monoenergetic Neutrons .....	24
IV.D. Measurement Results for Various Neutron Sources.....	28
IV.E. Pulse Shape Discrimination for BC-523A .....	30
IV.F. Measurement Results and Analysis.....	31
IV.G. Conclusions.....	34
IV.H. References.....	35
V. ASSESSMENT OF ELPASOLITE SCINTILLATORS WITH NEUTRON/GAMMA DISCRIMINATION AS THE BASIS FOR A HYBRID PASSIVE ENRICHMENT METER SYSTEM.....	36
V.A. Introduction .....	36
V.B. Combining Passive Enrichment Techniques .....	36
V.C. Conclusions .....	37
V.D. References .....	37
VI. USE OF SPECIFIC THICK TARGET ALPHA PARTICLE INDUCED REACTION GAMMA RAY YIELDS FOR VARIOUS NUCLIDES IN URANIUM HEXAFLUORIDE AS A WAY TO ESTIMATE <sup>234</sup> U ABUNDANCE .....	38
VI.A. Abstract.....	38
VI.B. Introduction.....	38
VI.C. Background .....	39
VI.D. Method.....	40
VI.E. Analysis.....	40

VI.F. Experimental Results.....	41
VI.G. Discussion.....	43
VI.H. Future Work.....	44
VI.I. Conclusions.....	44
VI.J. References.....	45
VII. ELECTROMAGNETIC AND ACOUSTIC NDE TECHNIQUES TO AID IN UF <sub>6</sub> ENRICHMENT VERIFICATION .....	46
VII.A. Introduction .....	46
VII.B. Potential Application of Acoustic and Electromagnetic Techniques to Assist with NDA Measurements of UF <sub>6</sub> .....	47
VII.C. Conclusions.....	48
VII.D. References .....	49

## I. INTRODUCTION

Nondestructive assay (NDA) measurements of uranium cylinders play an important role in helping the International Atomic Energy Agency (IAEA) safeguard uranium enrichment plants. Traditionally, these measurements have consisted of a scale or load cell to determine the mass of  $\text{UF}_6$  in the cylinder combined with a gamma-ray measurement of the 186 keV peak from  $^{235}\text{U}$  to determine enrichment. More recently, Los Alamos National Laboratory (LANL) and Pacific Northwest National Laboratory (PNNL) have developed systems that exploit the passive neutron signal from  $\text{UF}_6$  to determine uranium mass and/or enrichment. These include the Uranium Cylinder Assay System (UCAS), the Passive Neutron Enrichment Meter (PNEM), and the Hybrid Enrichment Verification Array (HEVA). The purpose of this report is to provide the IAEA with new ideas on technologies that may or may not be under active development but could be useful for  $\text{UF}_6$  cylinder assay.

To begin, we have included two feasibility studies of active interrogation techniques. There is a long history of active interrogation in the field of nuclear safeguards, especially for uranium assay. Both of the active techniques provide a direct measure of  $^{235}\text{U}$  content. The first is an active neutron method based on the existing PNEM design that uses a correlated  $^{252}\text{Cf}$  interrogation source. This technique shows great promise for  $\text{UF}_6$  cylinder assay and is based on advanced technology that could be implemented in the field in the near term. The second active technique is nuclear resonance fluorescence (NRF). In the NRF technique, a bremsstrahlung photon beam could be used to illuminate the cylinder, and high-resolution gamma-ray detectors would detect the characteristic de-excitation photons. The results of the feasibility study show that under certain measurement geometries, NRF is impractical for  $\text{UF}_6$  cylinder assay, but the “grazing transmission” and “secant transmission” geometries have more potential for this application and should be assessed quantitatively.

The next set of techniques leverage scintillator detectors that are sensitive to both neutron and gamma radiation. The first is the BC-523A capture-gated organic liquid scintillator. The detector response from several different neutron energies has been characterized and is included in the study. The BC-523A has not yet been tested with  $\text{UF}_6$  cylinders, but the application appears to be well suited for this technology. The second detector type is a relatively new inorganic scintillator called CLYC. CLYC provides a complementary detection approach to the HEVA and PNEM systems that could be used to determine uranium enrichment in  $\text{UF}_6$  cylinders. In this section, the conceptual idea for an integrated CLYC-HEVA/PNEM system is explored that could yield more precision and robustness against systemic uncertainties than any one of the systems by itself.

This is followed by a feasibility study on using alpha-particle-induced reaction gamma-rays as a way to estimate  $^{234}\text{U}$  abundance in  $\text{UF}_6$ . Until now, there has been no readily available estimate of the strength of these reaction gamma-rays. Thick target yields of the chief reaction gammas are computed and show that they are too weak for practical safeguards applications. In special circumstances where long count times are permissible, the 1,275 keV  $\text{F}(\alpha, \gamma)$  is observable. Its strength could help verify an operator declaration provided other knowledge is available (especially the age). The other  $\text{F}(\alpha, \gamma)$  lines are concealed by the dominant uranium line spectrum and associated continuum.

Finally, the last section provides several ideas for electromagnetic and acoustic nondestructive evaluation (NDE) techniques. These can be used to measure cylinder wall thickness, which is a source of systematic uncertainty for gamma-ray-based NDA techniques; characterize the UF<sub>6</sub> filling profile inside the cylinder, which is a source of systematic uncertainty for neutron-based NDA techniques; locate hidden objects inside the cylinder; and provide a unique identification of cylinders. Acoustic and electromagnetic NDE techniques are complementary to NDA measurements, and may improve the accuracy and continuity of knowledge of UF<sub>6</sub> measurements of interest to the IAEA.

As concepts and approaches for enrichment plant safeguards continue to evolve to meet modern challenges, the conceptual ideas explored in this report, along with more traditional techniques, help define the toolkit of technologies available for UF<sub>6</sub> cylinder assay. Whether the application is an unattended cylinder verification station or an on-site inspection, the basic building blocks can be tailored to provide the best solution given competing constraints such as size and weight limitations, required precision, mechanical complexity, cost, stability, robustness, etc. Many of the tools provide complementary information that can be combined in various ways to address unique, facility-specific measurement needs. Continued research in this area will ultimately help the international safeguards community to develop flexible solutions to enrichment plant safeguards challenges that meet the needs of the IAEA while placing the minimum burden on facility operators.

## II. MONTE CARLO FEASIBILITY STUDY OF AN ACTIVE NEUTRON ASSAY TECHNIQUE FOR UF<sub>6</sub> CYLINDERS USING A CORRELATED INTERROGATION SOURCE

*Karen A. Miller, Howard O. Menlove, Martyn T. Swinhoe, Johnna B. Marlow  
Los Alamos National Laboratory*

### II.A. Abstract

Uranium cylinder assay plays an important role in the nuclear material accounting at gas centrifuge enrichment plants. The Passive Neutron Enrichment Meter (PNEM) was designed to determine uranium mass and enrichment in 30B and 48Y cylinders using total neutron and coincidence counting in the passive mode. In this paper, we report the results of a Monte-Carlo-based feasibility study for an active uranium cylinder assay system based on the PNEM design. There are many advantages of the active technique such as a shortened count time and a more direct measure of <sup>235</sup>U content. The active system is based on a modified PNEM design and uses a <sup>252</sup>Cf source as the correlated active interrogation source. We show through comparison with a random AmLi source of equal strength how the use of a correlated driver significantly boosts the active signal and reduces the statistical uncertainty. We also discuss ways in which an active uranium cylinder assay system can be optimized to minimize background from <sup>238</sup>U fast-neutron induced fission and direct counts from the interrogation source. Based on the results of the feasibility study, we believe that this technology shows great promise and should be explored further in sensitivity studies and field testing.

### II.B. Introduction

In the field of nuclear safeguards, material accounting is used to track the inventory and flow of nuclear materials throughout the fuel cycle. As the most immediate tool to detect the diversion of nuclear material, it serves as the first line of defense against proliferation. The nuclear material used in gas centrifuge enrichment plants is in the form of uranium hexafluoride (UF<sub>6</sub>). At any given time, the majority of the UF<sub>6</sub> at an enrichment plant is contained in 30B and 48Y storage cylinders, so accurate uranium cylinder verification techniques are critical for verifying the uranium inventory at an enrichment plant.

Over the past several years, two neutron-based systems for UF<sub>6</sub> cylinder assay have been developed at Los Alamos National Laboratory (LANL). These are the Uranium Cylinder Assay System (UCAS) [1], which is installed at Rokkasho Enrichment Plant in Japan, and the Passive Neutron Enrichment Meter (PNEM) [2]. Pacific Northwest National Laboratory (PNNL) has also been developing a system for UF<sub>6</sub> cylinder assay called the Hybrid Enrichment Verification Array (HEVA) [3], which measures the neutron-induced gamma signal from the cylinder wall. Something that all three of these systems have in common is that they rely on passive neutron interactions to determine the <sup>235</sup>U mass (UCAS), enrichment (HEVA), or both mass and enrichment (PNEM) in the cylinder. The neutrons come primarily from F(α,n) reactions from the alpha-decay of <sup>234</sup>U and <sup>238</sup>U as well as spontaneous fission in <sup>238</sup>U, although the PNEM system also measures induced fission in <sup>235</sup>U from the thermal-neutron albedo.

One of the drawbacks of these methods is that they use indirect measures of <sup>235</sup>U content that rely on *a priori* knowledge of the <sup>234</sup>U/<sup>235</sup>U ratio. In commercial gas centrifuge enrichment plants, the <sup>234</sup>U content is constrained by two ASTM standards, and the <sup>234</sup>U/<sup>235</sup>U ratio is

typically very predictable. However, there may be cases where perturbations in the minor uranium isotopes may affect the accuracy of passive neutron measurement techniques such as reprocessed UF<sub>6</sub>, re-enriched tails, and highly-enriched uranium (HEU) downblending.

With these issues in mind, we conducted a Monte-Carlo-based feasibility study of an active neutron system for UF<sub>6</sub> cylinder assay based on the PNEM design. There is a long history of active nondestructive assay techniques for safeguards applications, especially for uranium measurements. They have been successfully applied in instruments such as the Active Well Coincidence Counter (AWCC) [4], the Neutron Coincidence Collar for fresh fuel assay [5], and the Advanced Experimental Fuel Counter (AEFC) for research reactor spent fuel measurements [6]. Active measurements of UF<sub>6</sub> cylinders were demonstrated in 1973 by Walton using an AmLi interrogation source and <sup>4</sup>He proportional counters (fast neutron detectors) [7]. This system used total neutron counting. A similar system called Contrôleur Isotopique Non-Destructif (CIND) has been used by Euratom for UF<sub>6</sub> cylinder assay at enrichment plants [8].

The principle behind active measurements is to use an external neutron source to induce fission in the assay object, which is the UF<sub>6</sub> in the cylinder in this case. In order to distinguish induced fission from spontaneous fission neutrons, the passive Doubles count rates from the assay object ( $D_{passive}$ ) and the interrogation source ( $D_{src}$ ) are subtracted from the active Doubles count rate ( $D_{active}$ ) to get the Net Doubles count rate ( $D_{net}$ ) as shown in Eq. 1.

$$D_{net} = D_{active} - D_{passive} - D_{src} \quad (1)$$

Traditionally, sources that emit random neutrons such as AmLi have been used as active drivers so that the interrogation source itself does not add to the Doubles background; however, AmLi sources are no longer being manufactured. Recently, LANL developed a concept for active interrogation that uses <sup>252</sup>Cf, a spontaneous fission source, as an active interrogation source. The technique was successfully implemented in the recent AEFC spent fuel measurements in Uzbekistan [9]. In order to minimize the Doubles background from <sup>252</sup>Cf, the interrogation source must be de-coupled from the detectors while being highly coupled to the assay object. Because the <sup>252</sup>Cf interrogation source emits a burst of 3.76 neutrons on average, there is a chance that more than one neutron from the same spontaneous fission event will induce a fission event in the assay object in the same coincidence time gate. The neutrons emitted from these induced fissions are correlated in time by the same spontaneous fission birth event, and the net result is to provide an increase in the effective multiplicity of the induced fission events seen by the detector in the coincidence time gate. The time gates for coincidence counting are determined by the neutron die-away time of the detector system as well as the neutron die-away time in the sample interrogation region. The PNEM detector pods have a die-away time of about 35  $\mu$ s.

In this paper, we present the results of our feasibility study for an active neutron technique for UF<sub>6</sub> cylinder assay. The superior performance of using <sup>252</sup>Cf as the interrogation source in Doubles mode compared to an AmLi source with the same neutron emission rate is illustrated with modeling results. The significance of an active neutron assay technique is that it can provide a direct measurement of <sup>235</sup>U content in UF<sub>6</sub> cylinders that is independent of variations in <sup>234</sup>U content, prior reactor history, enrichment method, high neutron background rates, and uncertainty in F( $\alpha$ ,n) yields, and the count time to achieve 1% statistics on the Net Doubles count rate is significantly smaller than comparable passive or AmLi-based active Doubles methods.



## II.C. Monte Carlo Modeling

The active neutron uranium cylinder assay technique was modeled using Monte Carlo N-Particle Extended (MCNPX) [10]. The design for the system was based on the existing PNEM with 4-atmosphere  $^3\text{He}$  tubes. Photographs of the PNEM system with a 30B cylinder at Rokkasho Enrichment Plant in Japan are shown in Fig. 1. The passive system consists of two briefcase-sized detector pods. Each pod has twelve  $^3\text{He}$  tubes embedded in a polyethylene slab. The slabs sit on the floor on both sides of the cylinder as shown in Fig. 1.



**Fig. 1. Photographs of the passive system with a 30B cylinder at Rokkasho Enrichment Plant.**

For the modeling of the active system, we added a polyethylene source holder with dimensions of 180 mm x 180 mm x 90 mm. The block was positioned directly underneath the cylinder, and the interrogation source was 10 mm deep in the polyethylene. This allows the interrogation source to be highly coupled to the  $\text{UF}_6$  cylinder but shielded from the detectors. A MCNPX rendering of the active system is shown in Fig. 2. For the feasibility study, we considered a full 30B cylinder. The  $\text{UF}_6$  was distributed as an annulus on the cylinder walls, which is consistent with filling by desublimation. We modeled  $\text{UF}_6$  with enrichment levels of zero to 5%  $^{235}\text{U}$ . The isotopics for each enrichment case are given in Table 1. For the zero percent enriched case, the uranium was modeled as 100%  $^{238}\text{U}$ . We modeled active systems with AmLi and  $^{252}\text{Cf}$  interrogation sources with neutron emission rates of  $5 \times 10^4$  n/s. In order to model the passive measurements, we used the  $F(\alpha, n)$  and spontaneous fission specific yields given in Table 2.

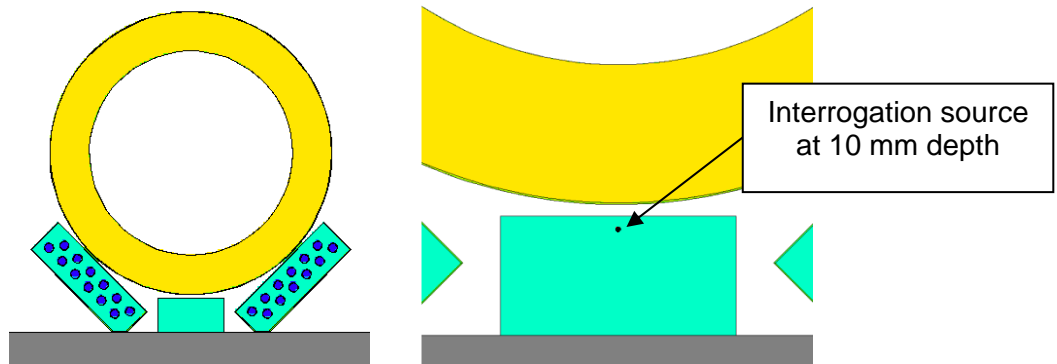


**Fig. 2. MCNPX rendering of the active system showing the two detector pods, a polyethylene source holder, and a full 30B cylinder with  $\text{UF}_6$  distributed on the cylinder walls.**

**Table 1. Uranium Isotopics for Low-Enriched UF<sub>6</sub>.**

<sup>234</sup> U [%]	<sup>235</sup> U [%]	<sup>238</sup> U [%]
0.00781	1.0	98.99219
0.01665	2.0	97.98335
0.02549	3.0	96.97451
0.03433	4.0	95.96567
0.04317	5.0	94.95683

**Table 2. Specific Neutron Yields in UF<sub>6</sub> from F(α,n) and Spontaneous Fission Reactions.**

Isotope	F(α,n) [n/s/g]	Spontaneous Fission [n/s/g]
<sup>234</sup> U	5.76E+02	5.02E-03
<sup>235</sup> U	8.80E-02	2.99E-04
<sup>238</sup> U	1.43E-02	1.36E-02

## II.D. Comparison of Random and Correlated Interrogation Sources

The modeling results are given in Table 3. The table provides the passive Singles and Doubles count rates for the range of enrichments. For the active measurements, the Net Singles and Doubles count rates are given, where the passive and interrogation source count rates are subtracted from the active count as shown in Eq. 1. The most significant results come from a comparison of the Net Doubles count rates for each technique. The Net Doubles with the AmLi source is very similar in size to the passive Doubles; however, the Net Doubles with the <sup>252</sup>Cf source is an order of magnitude larger than the passive Doubles.

The high Doubles count rate with <sup>252</sup>Cf demonstrates the concept that the use of a correlated interrogation source in an active interrogation method increases the effective multiplicity in the measured time gate. It also shows that the <sup>252</sup>Cf interrogation source can be sufficiently decoupled from the detectors while being highly coupled to the assay object.

**Table 3. Modeling Results for Passive and Active Cylinder Measurements.**

Enrichment [ <sup>235</sup> U%]	Passive		Active, AmLi Source		Active, <sup>252</sup> Cf Source	
	Singles [cps]	Doubles [cps]	Net Singles [cps]	Net Doubles [cps]	Net Singles [cps]	Net Doubles [cps]
0.0	865	33	1,553	0	2,055	594
1.0	2,539	67	3,012	136	3,186	1,281
2.0	4,498	130	3,683	219	3,690	1,731
3.0	6,528	196	4,067	290	4,022	2,074
4.0	8,745	288	4,385	344	4,276	2,349
5.0	10,960	383	4,630	392	4,475	2,584

A plot of the Net Doubles count rates for the AmLi and <sup>252</sup>Cf interrogation sources is shown in Fig. 3. One feature to note is that the <sup>252</sup>Cf interrogation source does not cross the y-axis at the

origin. This is due to the contribution from fast-neutron-induced fission in  $^{238}\text{U}$ . Although the cross section for thermal-neutron-induced fission in  $^{235}\text{U}$  is about 100 times larger than fast-neutron-induced fission in  $^{238}\text{U}$ , low-enriched  $\text{UF}_6$  contains about 30 times more  $^{238}\text{U}$  than  $^{235}\text{U}$ . In order to reduce the  $^{238}\text{U}$  fast fission contribution in an optimized system, the interrogation source should be positioned deeper in the polyethylene source holder to reduce the energy of the interrogation neutrons. The AmLi interrogation source has the advantage that there is no  $^{238}\text{U}$  induced fission component to the measured signal due to the fact that the AmLi neutrons are emitted with average energies of only 0.3 MeV (compared to 2.14 MeV for  $^{252}\text{Cf}$ ).

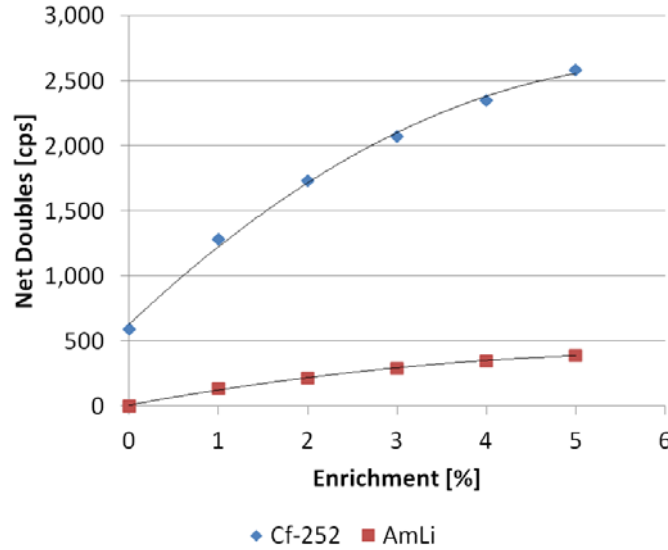


**Fig. 3. Net Doubles count rate for a 4-atm system using a  $^{252}\text{Cf}$  vs. AmLi active interrogation source assuming equal source strengths of  $5 \times 10^4$  n/s.**

Statistical uncertainty plays an important role in determining the suitability of a particular assay technique to the measurement scenario under consideration. Specifically, statistical uncertainty affects the count time to reach the desired precision. The statistical uncertainty in the Net Doubles rate ( $\sigma_{D,net}$ ) contains contributions from uncertainty in the active ( $\sigma_{D,active}$ ), passive ( $\sigma_{D,passive}$ ), and source ( $\sigma_{D,src}$ ) measurements and is given by Eq. 2.

$$\sigma_{D,net}^2 = \sigma_{D,active}^2 + \sigma_{D,passive}^2 + \sigma_{D,src}^2 \quad (2)$$

The statistical uncertainty in the Net Doubles rate is a function of the active and passive Doubles as well as the accidental ( $A$ ) pileup in the coincidence gate from the Singles count rate. The accidental rate is equal to the square of the Singles ( $S$ ) count rate multiplied by the gate length ( $G$ ):

$$A = S^2 G. \quad (3)$$

The uncertainty associated with each of the right-hand side terms in Eq. 2 is given by

$$\sigma_D = \frac{\sqrt{D + A}}{\sqrt{t}} \quad (4)$$

where  $t$  is the count time. In order to compare the statistical uncertainty associated with each interrogation source, we evaluated the uncertainty for the case of a full 30B cylinder containing 4% enriched  $\text{UF}_6$ , where the source strengths for both the  $^{252}\text{Cf}$  and AmLi sources is  $5 \times 10^4$  n/s and the gate length is 64  $\mu\text{s}$ . Table 4 contains the components in the error calculation for each method.

**Table 4. Active Methods Error Terms.**

<b>Component</b>	<b>Active [cps] <math>^{252}\text{Cf}</math> Source</b>	<b>Active [cps] AmLi Source</b>
$D_{\text{active}}$	2,444	344
$A_{\text{active}}$	13,035	12,339
$D_{\text{passive}}$	288	288
$A_{\text{passive}}$	4,894	4,894
$D_{\text{src}}$	95	0
$A_{\text{src}}$	100	37

Using the data contained in Table 4, we calculated the count times required to achieve 1% statistical precision on the Net Doubles for the  $^{252}\text{Cf}$  and AmLi sources. Recognizing that the direct Doubles contribution from the source does not need to be measured for each cylinder, we allowed for a 1,000-second source measurement for both cases, making the source uncertainty negligible. We also chose the combination of active and passive count times such that the error contributions were equal ( $\sigma_{D,\text{active}} = \sigma_{D,\text{passive}}$ ). Table 5 shows the breakdown of passive, active, and total count times required for the  $^{252}\text{Cf}$  and AmLi sources for this example. The total count time for the  $^{252}\text{Cf}$  method is 76 seconds compared to 3,066 seconds for the AmLi source. This example case clearly shows the statistical advantage of using a  $^{252}\text{Cf}$  interrogation source over an AmLi source.

**Table 5. Count Times to Achieve 1% Statistical Uncertainty on the Net Doubles.**

<b>Measurement</b>	<b><math>^{252}\text{Cf}</math> Source Count Time [seconds]</b>	<b>AmLi Source Count Time [seconds]</b>
Passive	19	876
Active	57	2,190
Total	76	3,066

Note that an active interrogation technique generally requires both a passive and an active measurement. Because the Doubles count rate in the active  $^{252}\text{Cf}$  measurement is so much larger than in the passive measurement, the uncertainty in the passive measurement becomes less significant in the Net Doubles count rate. With a modest increase in the yield of the  $^{252}\text{Cf}$  source, the passive background becomes rather negligible.

## **II.E. Detector Optimization**

In this section, we discuss some of the parameters that can be optimized for the active system using a correlated  $^{252}\text{Cf}$  interrogation source. First, the Net Doubles are a combination of the

induced fission in both the  $^{235}\text{U}$  and  $^{238}\text{U}$ , and we would like to minimize the  $^{238}\text{U}$  contribution. Because the induced fission in  $^{238}\text{U}$  comes from fast neutrons, the  $^{238}\text{U}$  induced fission rate is a function of the  $^{252}\text{Cf}$  depth in the polyethylene block moderator. As the source moves deeper into the polyethylene block, both the thermal-neutron  $^{235}\text{U}$  induced fission signal and the fast-neutron  $^{238}\text{U}$  induced fission background decrease. However, the  $^{238}\text{U}$  induced fission component decreases at a much faster rate than  $^{235}\text{U}$  induced fission. Fig. 4 shows a plot of the Net Doubles count rate as a function of enrichment for three different source depths of 10 mm, 30 mm, and 60 mm in the polyethylene moderator. The  $^{238}\text{U}$  induced fission component, represented by the y intercept, decreases the deeper the interrogation source is in the moderator.

Another design component that can be optimized is the strength of the interrogation source. A larger source strength will result in a larger active signal. This has to be balanced with the regulatory and health physics aspects of source handling. Table 6 provides a breakdown of the Doubles signals (Net, active, passive, and source) for all three source depths and source strengths of  $5 \times 10^4$  n/s and  $5 \times 10^5$  n/s assuming a full 30B cylinder with 4% enriched  $\text{UF}_6$ . The most important thing to note from Table 6 is the relative size of the passive and net signals for the two different source strengths. The passive signal is the same for every configuration listed in Table 6, but the magnitude of the Net Doubles count rate is highly dependent on the magnitude of the source strength. In the case of the  $5 \times 10^4$  n/s source, the Net Doubles count rate is one order of magnitude larger than the passive signal, but it is two orders of magnitude larger for the  $5 \times 10^5$  n/s source. The uncertainty associated with passive measurement becomes less important as the passive signal becomes a smaller portion of the overall active signal. With a  $5 \times 10^5$  n/s source, the passive measurement is not required.

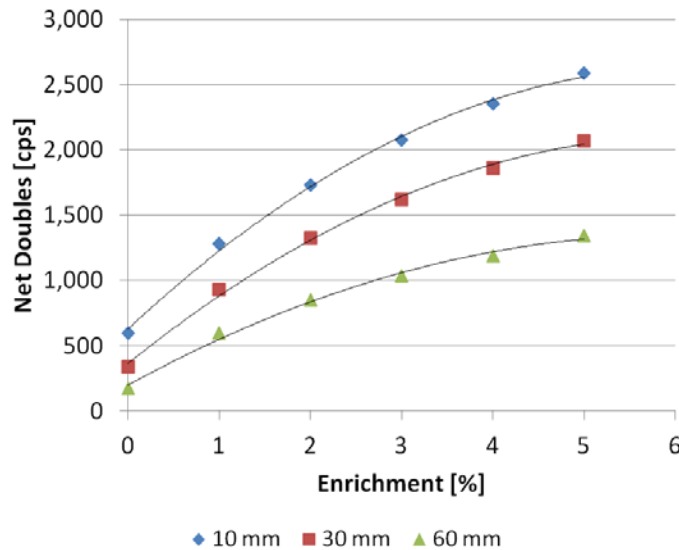


**Fig. 4. Net Doubles as a function of enrichment for three different  $5 \times 10^4$  n/s  $^{252}\text{Cf}$  source depths. The  $^{238}\text{U}$  induced fission background is reduced the deeper the source is positioned in the polyethylene block.**

**Table 6. Relative Doubles Contributions for Various Source Depth and Strength Combinations for a Full 30B Cylinder Containing 4% Enriched UF<sub>6</sub>.**

Source Depth [mm]	Source Strength [n/s]	D <sub>net</sub> [cps]	D <sub>active</sub> [cps]	D <sub>passive</sub> [cps]	D <sub>Cf</sub> [cps]
10	$5 \times 10^4$	2,349	2,732	288	95
30	$5 \times 10^4$	1,859	2,219	288	72
60	$5 \times 10^4$	1,190	1,576	288	98
10	$5 \times 10^5$	23,492	24,726	288	946
30	$5 \times 10^5$	18,587	19,592	288	717
60	$5 \times 10^5$	11,897	13,168	288	983

The design of the interrogation source moderator can also be optimized to minimize the source Doubles background. Table 6 shows that the source background is smallest for the case where the source is 30 mm deep in the moderator (the source background increases for the 60 mm depth due to neutrons scattering from the floor into the detector slab). Finally, the gas pressure of <sup>3</sup>He in the detector, which was modeled as 4-atmospheres for this study, can be optimized for various constraints such as count time or the supply of <sup>3</sup>He. For this feasibility study, we did not alter the moderator design or <sup>3</sup>He gas pressure, but along with the interrogation source strength and depth, an optimized design can be used to minimize sources of background in the active signal.

## II.F. Counting Statistics Projected onto Enrichment

In section 3, we showed how the uncertainty in the Net Doubles rate is calculated. In this section, we show how the statistical uncertainty in the Net Doubles projects onto statistical uncertainty in the enrichment determination. Using the optimization calculations from the previous section, we consider the system with a source depth of 30 mm and strength of  $5 \times 10^5$  n/s. The Net Doubles count rate as a function of enrichment is plotted in Fig. 5.

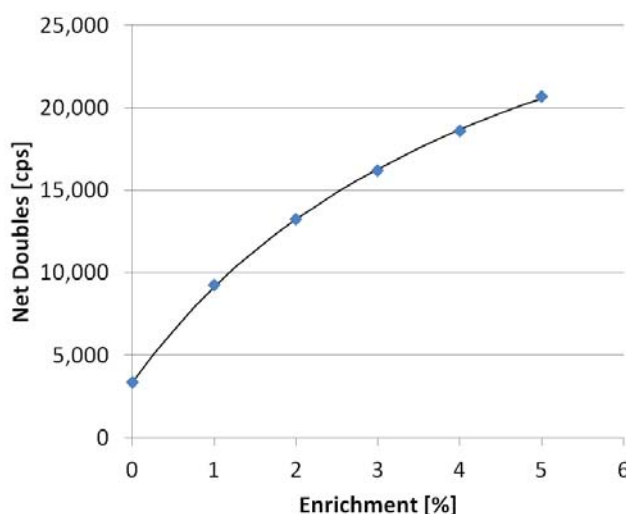


**Fig. 5. Net Doubles rate as a function of enrichment for a system with a source depth of 30 mm and strength of  $5 \times 10^5$  n/s.**

We assume the following functional form for the shape of the curve in Fig. 5.

$$D_{net} = \frac{ae}{1 + be} + c \quad (5)$$

where  $e$  is enrichment and  $a$ ,  $b$ , and  $c$  are constants. In practice, the constants are determined in calibration, and each constant has uncertainty associated with it. This results in systematic uncertainties that are not considered here. The slope of the curve is given by Eq. 6.

$$D'_{net} = \frac{a}{(1 + be)^2} \quad (6)$$

The slope evaluated at a point is equal to the ratio of the statistical uncertainty in the Net Doubles count rate to the statistical uncertainty in the enrichment. Thus, the uncertainty in the enrichment ( $\sigma_e$ ) can be calculated with Eq. 7.

$$\sigma_e = \frac{\sigma_{D,net}}{D'_{net}} \quad (7)$$

Assuming a passive count time of 20 seconds and an active count time of 60 seconds, we evaluated the statistical uncertainty in the Net Doubles count rate and how that projects onto statistical uncertainty in the enrichment determination. The results are plotted in Fig. 6, evaluated at 1%, 2%, 3%, 4%, and 5% enriched UF<sub>6</sub>. The uncertainty in the Net Doubles decreases as enrichment increases because it is based on the passive and active count rates, which increase with enrichment. The uncertainty in the enrichment dips in the middle of the range because it is a function of both count rates and the shape of the curve in Fig. 5. The Net count rate is smallest for lower enrichments, but the slope of the curve is steeper at lower enrichments (due to self-shielding effects). These two effects work in opposition and produce the enrichment uncertainty curve in Fig. 6.

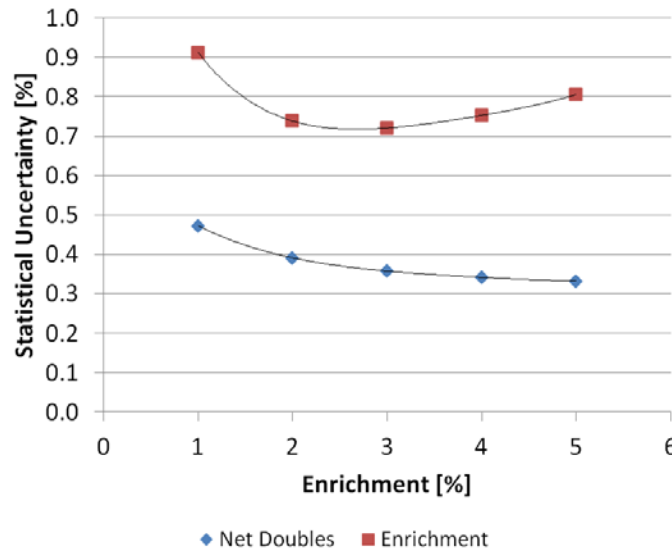


Fig. 6. Statistical uncertainty in the Net Doubles and enrichment as a function of enrichment.

Another feature of the plot in Fig. 6 is the fact that the statistical uncertainty in the enrichment is below 1% assuming a total count time of only 80 seconds. In this case, the contribution to the

error from the passive measurement is negligible compared to the active measurement. With a  $^{252}\text{Cf}$  source strength of  $5 \times 10^5$  n/s, the passive measurement is not necessary. This is especially important for unattended applications to avoid the necessity of a source movement.

## II.G. Conclusions

This feasibility study of an active neutron technique for  $\text{UF}_6$  cylinder assay shows that this type of system is a viable measurement technique for enrichment plant safeguards that should be explored in more detail. It has many advantages over a passive measurement technique including:

- It measures  $^{235}\text{U}$  content directly;
- It is independent of variations in  $^{234}\text{U}$  content from factors such as the enrichment method, re-enriched tails, and HEU downblending;
- It is independent of prior reactor history, meaning that it can be used to assay reprocessed  $\text{UF}_6$ ;
- It is independent of uncertainties in  $F(\alpha, n)$  neutron yields in uranium isotopes;
- It penetrates well beyond potential wall deposits of different enrichments;
- It is not sensitive to high neutron background rates; and
- The total count time can be approximately one minute.

We also showed a significant improvement in the active assay technique using a  $^{252}\text{Cf}$  correlated source as the active driver compared to an AmLi source. In addition to the improved performance, it is important because AmLi sources are no longer being manufactured. This result may also have carry-over effects for improved performance in other applications of active nondestructive assay.

Future work on this technique should be focused on optimization of the active design. Specifically, the design should balance factors such as the depth of the interrogation source in the moderator (to reduce  $^{238}\text{U}$  fast fission background), the strength of the  $^{252}\text{Cf}$  source (constrained by health physics regulations and licensing), the design of the polyethylene moderator for the source (to minimize the  $^{252}\text{Cf}$  background), and the efficiency of the detector pods.

In addition to optimization calculations, sensitivities studies should be performed to understand the effect of variation in the  $\text{UF}_6$  filling profile on the assay result. The authors have studied the variation in filling profiles of 30B and 48Y cylinders at Rokkasho Enrichment Plant in Japan and Westinghouse Fuel Fabrication Facility in Columbia, South Carolina, and little variation between cylinders was observed in most cases. Because the count time associated with the active  $^{252}\text{Cf}$  method is so short, variation in filling profiles could potentially be diagnosed by taking active measurements with the interrogation source in different positions relative to the cylinder. This would essentially turn the active interrogation method into a crude neutron imaging technique. This type of activity would likely not be used in unattended mode operation, but it may be useful in special circumstances of attended mode operation.

Finally, the technique should be tested in a field trial. This could be done using the existing PNEM detector pods. Agreements would need to be negotiated with enrichment or fuel fabrication plant operators. Because  $^{252}\text{Cf}$  is often used as a calibration or diagnostic source for neutron detectors, some enrichment plants may already have license and ownership of one at their facility. As shown in this feasibility study, an active neutron assay technique for  $\text{UF}_6$



cylinders has the potential to be an important tool for enrichment plant safeguards and should be further studied to understand its capabilities and limitations.

## II.H. References

1. K.A. Miller, M.T. Swinhoe, J.B. Marlow, H.O. Menlove, C.D. Rael, T. Iwamoto, T. Tamura, S. Auichi, *J. Nucl. Mat. Manag.*, **39**, 1 (2010).
2. K.A. Miller, H.O. Menlove, M.T. Swinhoe, and J.B. Marlow, *ESARDA Bull.*, **46** (2011).
3. L.E. Smith, E.K. Mace, A.C. Misner, and M.W. Shaver, *IEEE Trans. Nucl. Sci.*, **57**, 4, 2247-2253 (2010).
4. H.O. Menlove, LA-7823-M, Los Alamos National Laboratory Manual (1979).
5. H.O. Menlove, LA-8939-M, Los Alamos National Laboratory Manual (1981).
6. H.O. Menlove, M.T. Swinhoe, J.B. Marlow, C.D. Rael, LA-14359, Los Alamos National Laboratory Manual (2008).
7. R.B. Walton, T.D. Reilly, J.L. Parker, J.H. Menzel, E.D. Marshall, L.W. Fields, *Nucl. Tech.*, **21**, 133-148 (1973).
8. R.A. Picard, proc. ESARDA Annual Meeting, Versailles, France, 265-269 (1983).
9. H. Menlove, J. Marlow, K. Miller, C. Rael, M. Swinhoe, W. O'Connor, T. Sobolev, R. Zarucki, A. Lebrun, E. Van Schijndel, U. Yavuz, U. Salikhbaev, S. Baytelesov, S. Alikulov, A. Boltabaev, proc. INMM Annual Meeting, Orlando, Florida (2012). (to be published)
10. D.B. Pelowitz, J.S. Hendricks, J.W. Durkee, M.R. James, M.L. Fensin, G.W. McKinney, S.G. Mashnik, L.S. Waters, LA-UR 08-07182, Los Alamos National Laboratory Report (2008).

### III. FEASIBILITY ASSESSMENT OF APPLICATION OF NUCLEAR RESONANCE FLUORESCENCE TO ACTIVE UF<sub>6</sub> CYLINDER ENRICHMENT ASSAY

*Glen A. Warren, Jac Caggiano, Patrick Peplowski, David V. Jordan*  
*Pacific Northwest National Laboratory*

#### III.A. Introduction

Nuclear resonance fluorescence (NRF) is a well-established and well-understood physical process [1,2] that can be applied to isotope-specific detection, characterization, and non-destructive assay (NDA) of interrogated samples [3]. NRF refers to the nuclear absorption of photons (typically  $O(1-10 \text{ MeV})$ ) at discrete energy levels, followed by the electromagnetic de-excitation of the excited nucleus (see Figure 1). Through that process, one or more photons are emitted roughly isotropically. The energies of the emitted photons are characteristic of the individual isotopes of the element. This unique information provides a means to identify specific isotopes, either stable or radioactive. A bremsstrahlung photon beam (generated by e.g. a linear accelerator or other electron source) is typically used to illuminate the sample, and high-resolution gamma-ray detectors (typically high-purity germanium (HPGe)) detect the de-excitation photons. Depending upon the measurement geometry, the NRF signature can consist of either the de-excitation photons from stimulated nuclei in the target, or depletion of the incident photon beam at the characteristic absorption energies for stimulation of the relevant nuclear levels.

The application of NRF to assay of uranium enrichment in UF<sub>6</sub> cylinders suggests itself as a potentially attractive, active-interrogation alternative to passive assay methods for the following reasons:

- The isotope-specific interrogation method probes the <sup>235</sup>U content of the inspected material volume, yielding a response metric that scales with the <sup>235</sup>U mass. In contrast to passive neutron-based signatures, which rely upon a known (e.g. via calibration) correlation between <sup>234</sup>U and <sup>235</sup>U isotopic abundances in the enriched product, a “direct” measure of <sup>235</sup>U isotopic abundance may be more robust against variations in minor isotopic composition of feed stock and/or enrichment cascade performance.
- The energies of the interrogating photon beam and <sup>235</sup>U response-signature gamma-ray emissions are of order several MeV, rather than 186 keV for the emission line exploited in the traditional enrichment meter method. The attenuation length at 1733 keV, the strongest NRF line of <sup>235</sup>U, is about 4 cm in solid UF<sub>6</sub>, an order of magnitude larger than that of the 186-keV line [4]. This offers substantially greater effective assay depth and robustness against content inhomogeneities than the enrichment meter method, although it does not sample the entire UF<sub>6</sub> volume, as do neutron-based passive signatures. Note that a penetration depth on the order of centimeters means that the potential also exists for spectroscopic detection of anomalies in container form factor, e.g. “container-within-container” diversion scenarios.

Significant practical challenges to implementing the technique include (but are not necessarily limited to) the following:

- Significantly greater complexity, footprint, and expense in the inspection infrastructure and equipment relative to passive handheld-detector or portal-monitor approaches,

including the requirement to field and/or install an appropriately compact bremsstrahlung photon source and an array of high-resolution (e.g. HPGe) detectors.

- Large backgrounds and correspondingly low signal-to-noise ratios induced by illuminating a relatively massive  $\text{UF}_6$  cylinder with a broad-beam photon source.
- Dose-rate and equipment assay exclusion-zone concerns for enrichment facility workers and inspectors.

With these opportunities and challenges in mind, Pacific Northwest National Laboratory (PNNL) assessed the feasibility of applying NRF to the enrichment assay of  $\text{UF}_6$  cylinders [4]. The research was carried out as a task under National Nuclear Security Administration (NNSA) funding (Office of Nonproliferation Research and Development, NA-22) as part of a larger project lifecycle at PNNL aimed at investigating NRF signature science and applications to nuclear nonproliferation. The feasibility assessment took into account the following ingredients:

- Measured NRF signal rates from  $^{235}\text{U}$  (in thin-target geometry);
- Results of a measurement campaign on depleted uranium (DU) in slab geometry to aid in quantifying backgrounds and signal-to-noise;
- Analytical and Monte Carlo simulations of the NRF signal anticipated from interrogation of  $\text{UF}_6$  cylinders containing a range of product enrichments, from low-enriched uranium (LEU) to highly-enriched uranium (HEU), and incorporating typical material geometries and container form factors;
- Experiment-based assessments of collimated HPGe detector count-rate limitations (i.e., dead-times) under realistic measurement conditions.

This concept summary provides a very brief overview of the feasibility assessment at a level of detail sufficient to suggest the main ideas and conclusions; further details can be found in [4].

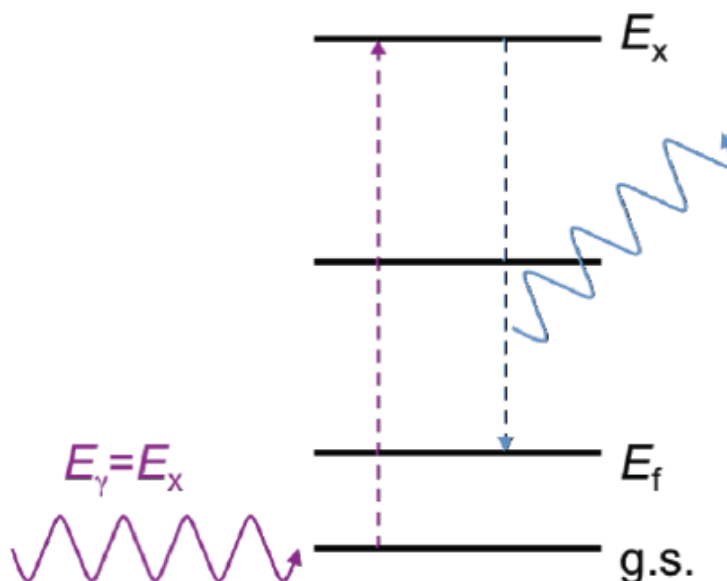


**Figure 1. Schematic of NRF process showing a typical nuclear level diagram, absorption of the interrogating photon, and emission of a de-excitation photon.**

### III.B. Feasibility Assessment

Figure 2 illustrates in schematic form the layout of a typical NRF measurement system. The system comprises a collimated bremsstrahlung photon beam, the target sample (a small slab of material in this illustration, but the concept generalizes to larger target form factors, e.g. a  $\text{UF}_6$  cylinder), and one or more gamma-ray detectors. Two main types of measurement are possible in principle: (1) For “scattering mode” measurements, a spectroscopic gamma-ray detector or detector array is positioned at finite scattering angle with respect to the incident photon beam direction, in order to measure the de-excitation gamma-rays depicted in Figure 1. (2) For “transmission mode” measurements, a secondary, isotopically-pure target matching the assay isotope of interest is positioned downstream of the interrogated sample. A detector views NRF emissions from this secondary target, with the goal of registering *depletion* of the incident beam at the energies specific to the isotope of interest: Occurrence of NRF in the inspected sample will preferentially deplete the beam at the relevant energies, leading to a drop (or “notch”) in the corresponding NRF signal from the secondary target. Either (or both) types of NRF measurement geometry can be incorporated in a single system; the two techniques are subject to somewhat different classes of statistical and systematic uncertainty. In either case, the relevant isotopic observable in the application of NRF to  $\text{UF}_6$  cylinder enrichment assay is the total  $^{235}\text{U}$  response from the portion of the cylinder contents illuminated by the interrogating photon beam.

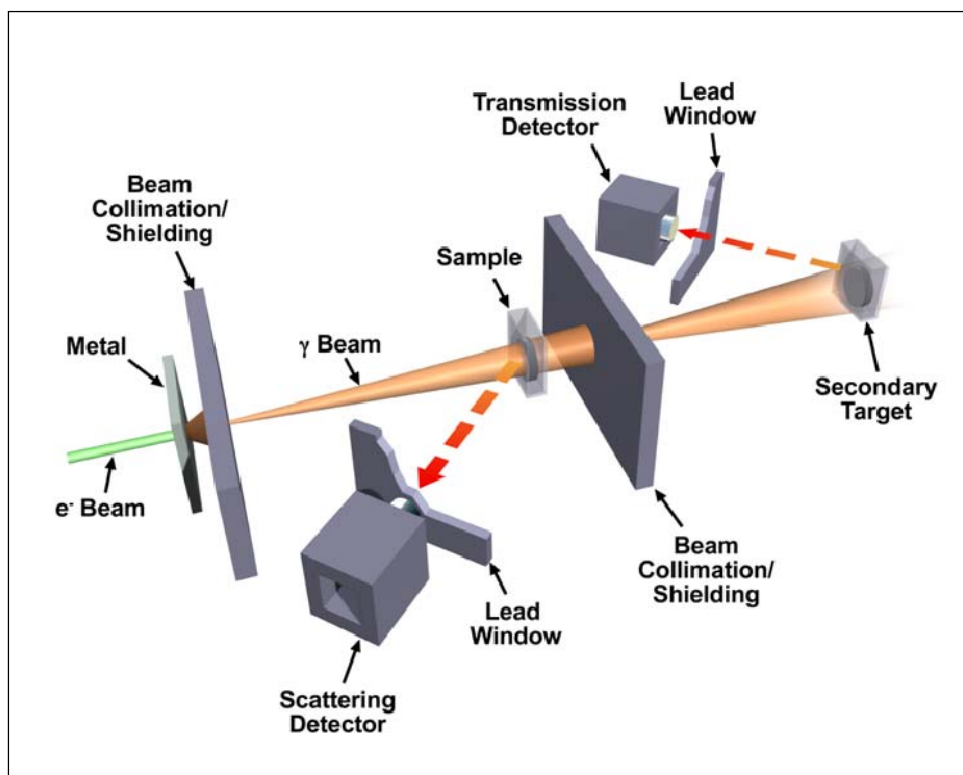


Figure 2. Diagram showing both scattering-mode and transmission-mode measurement geometries in a notional NRF system. The photon beam is generated through bremsstrahlung of an electron beam originating from the left of the diagram and illuminates the sample. For scattering-mode measurements, a collimated detector (positioned at a “backward” angle in this diagram) views the sample at finite scattering angle. For transmission-mode measurements, a collimated detector views a secondary target consisting of the isotopic component of interest in the sample.

Figure 3 below [5] illustrates the  $^{235}\text{U}$  NRF signal-response measured with a 100% relative efficiency HPGe detector in scattering-angle mode. The measurements were carried out by PNNL in collaboration with Passport Systems at the Massachusetts Institute of Technology (MIT) High-voltage Research Laboratory (HVRL) with a 2.8-MeV bremsstrahlung photon beam. The HEU target consisted of several foils (total thickness of order several mm) stacked into a plastic container. The prominent emission line at 1733 keV is indicated in the figure. The figure also suggests the qualitative shape of the continuum background in the region of the  $^{235}\text{U}$  NRF lines. PNNL investigated the intensity of this background, and the NRF signal-to-noise ratio as a function of areal target density, in various thick-slab DU target geometries. These background-characterization measurements, in tandem with the measured  $^{235}\text{U}$  NRF intensities, were subsequently applied as both NRF response-model validation cases and as bases for scaling the HPGe detector-system responses from slab-target geometry to the  $\text{UF}_6$  cylinder target geometries of interest. Further details of the various measurement campaigns on HEU and DU targets are available in [4,5,6].

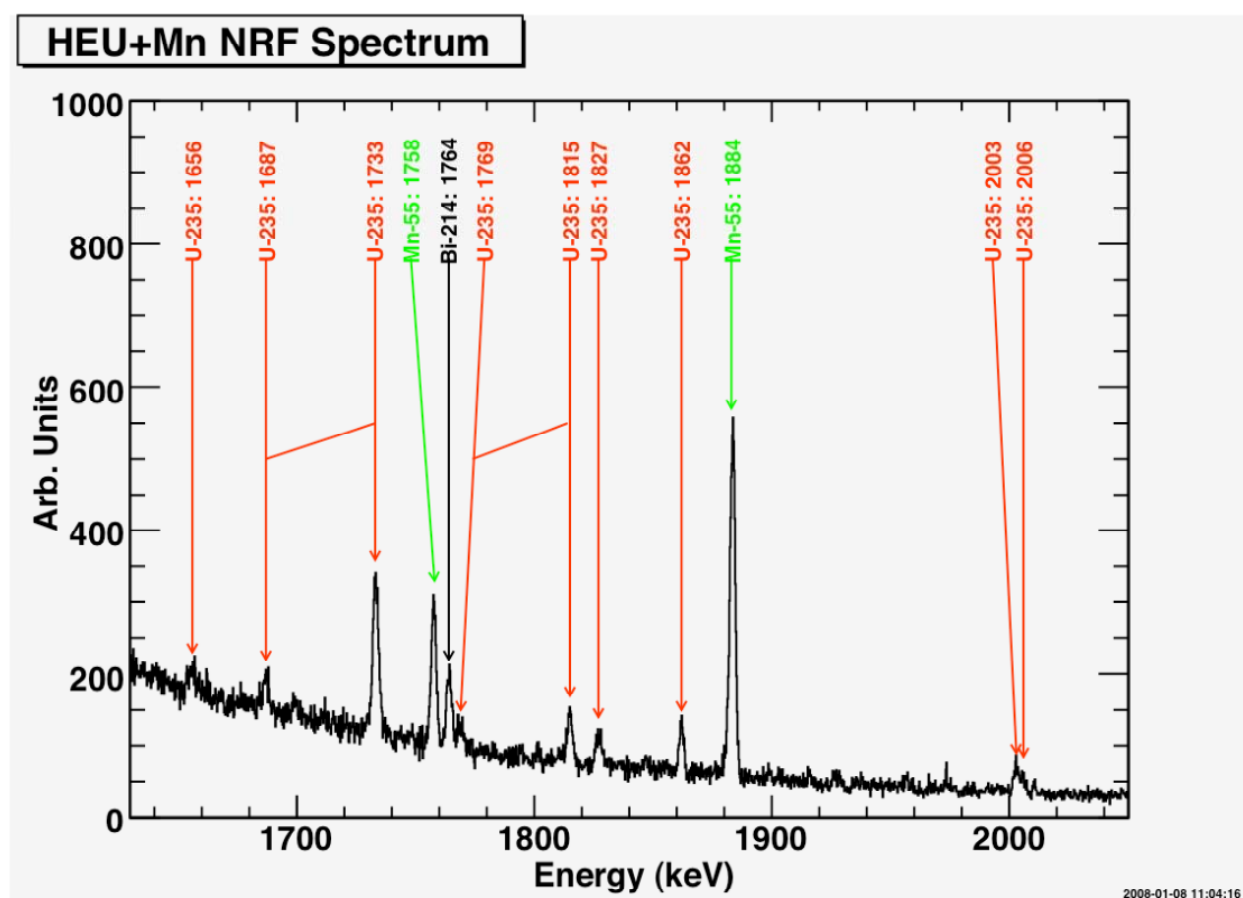


Figure 3. Measured NRF spectrum in finite scattering-angle mode on a relatively thin (*O*(several mm) thickness) HEU + Mn target [5].

A crucial challenge facing enrichment assay in  $\text{UF}_6$  cylinders containing LEU is the measurement of small quantities of  $^{235}\text{U}$  mixed with significantly larger quantities of other high-Z materials (e.g.,  $^{238}\text{U}$ ). The NRF background under the resonant peak is heavily dominated by

the response from the material with the largest atomic number ( $Z$ ) in the sample. The background is thus independent of isotopic enrichment. The  $^{235}\text{U}$  signal strength, and thus the signal-to-noise ratio, will therefore scale with the enrichment.

An analytical signal rate model of the scattering-mode NRF measurement approach was applied to evaluate the time required to determine the enrichment of a  $\text{UF}_6$  cylinder for various levels of enrichment. For a given signal-to-noise ratio,  $\alpha$ , and a specified relative uncertainty of the gamma-ray peak,  $r$ , the signal counts required are

$$S_{\text{req}} = \frac{1}{r^2} \frac{\alpha + 2}{\alpha}$$

For example, for  $r = 0.05$  and  $\alpha = 1$ ,  $S_{\text{req}} = 1.2 \times 10^3$ , whereas for  $\alpha = 0.1$ ,  $S_{\text{req}} = 8.4 \times 10^3$ . The signal-to-noise ratio for  $\text{UF}_6$  cylinder measurements was estimated by appropriately scaling the observed signal-to-noise of PNNL measurements on a target sample consisting of plates of 1.3-cm steel plus 2-cm DU. The expected signal-to-noise is 0.02:1 for 1% sample enrichment. The signal rate was calculated in a similar manner: scaling the observed rates on DU by a ratio of the analytical models. Figure 4 displays the calculation results, shown as time required for a 5% measurement. Note the log scale of the vertical axis.

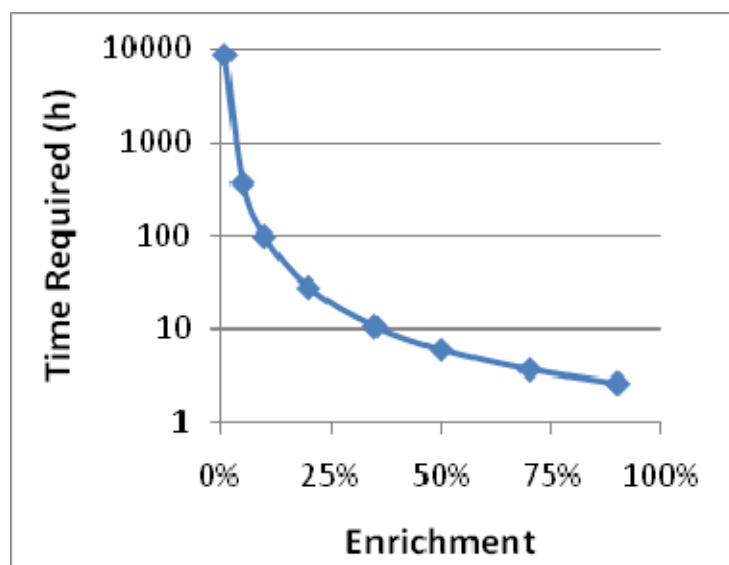


**Figure 4. Calculated dwell time required for a 5% (relative precision) measurement of the content of  $^{235}\text{U}$  in a  $\text{UF}_6$  cylinder via NRF “scattering mode” assay. An assay system consisting of four HPGe detectors, each of about 100% relative efficiency, is assumed. The system dead time is background-rate limited (independent of target enrichment) and assumed to be roughly 15%, comparable to experience gained in actual measurements on DU carried out in slab-target geometry.**

This result shows that measurement times for the scenario envisioned are in excess of 400 hours. The dwell times shown in the figure depend upon model-based extrapolation of signal rates and signal-to-noise ratios obtained in measurements using a DU slab target. Improvements in the measurement methodology could yield shorter time requirements, so it is worthwhile examining where possible improvements could be made.

There are a number of possible avenues to shortening the measurement times. Four roughly 100% relative-efficiency HPGe detectors were used for the measurements. By increasing the number of detectors, one could increase the signal rate. A tripling of the number of detectors

would then reduce the measurement times by a factor of three. One could also run at higher accelerator currents (i.e. higher interrogating photon-beam flux), which would increase detector rates. The detectors were typically run at 15% dead time in the DU-slab measurements, which is a reasonable value for a physics-driven measurement. For assay applications, however, the detectors can be driven at considerably higher event rates, which may provide up to a factor-of-two improvement in signal rate. No significant gain can be obtained by adjusting the measurement geometry because the measurements are detector rate limited. Thus, for a bremsstrahlung system, one might be able to reduce the measurement times by a factor of six. However, even with this reduction the estimated measurement times are still almost three orders of magnitude larger than typical passive-assay measurement times yielding comparable assay precision.

These assessments have focused on measurements of the NRF signal in finite-angle scattering mode. Given the evident limitations of this measurement approach for practical enrichment assay, it is worthwhile exploring transmission measurement concepts. The density of solid  $\text{UF}_6$  is approximately  $5 \text{ g/cm}^3$ , so that a 30B cylinder would present  $380 \text{ g/cm}^2$  (areal density) of material for a probe beam path coinciding with a cylinder diameter below the fill level (see Figure 5, red arrow). As discussed in [7], transmission measurements for NRF strengths comparable to the 1733-keV line of  $^{235}\text{U}$  lose sensitivity for sample thicknesses greater than  $100 \text{ g/cm}^2$  because of attenuation of the photon beam. Thus, transmission measurements through the center of the cylinder are not possible. It might be possible, however, to conduct a transmission measurement along a secant (Figure 5, orange arrow) so that the beam passes through only about  $100 \text{ g/cm}^2$  of material, or 20 cm. The disadvantage of that approach is that one would only be able to probe a relatively limited portion of the  $\text{UF}_6$  volume, and the amount of material sampled would depend upon fill depth. However, a sample-path length on the order of 10 cm is still an order of magnitude larger than the infinite-thickness criterion, 1.4 cm, at 186-keV in the traditional enrichment meter method [8]. A secant path near the bottom of the cylinder (Figure 5, black arrow) would similarly limit attenuation losses, but might be inordinately susceptible to the possible presence of “heels” at the cylinder bottom.

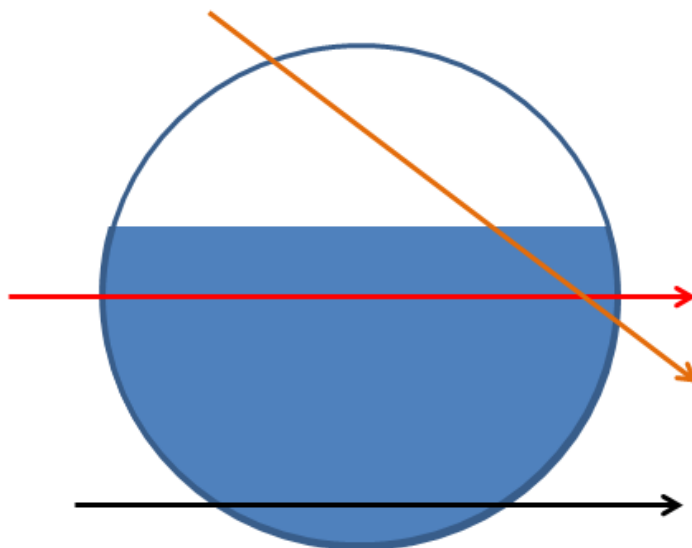


**Figure 5. Cross-section of  $\text{UF}_6$  cylinder at approximately 60% fill illustrating candidate probe photon beam trajectories for NRF transmission measurements.**

As a final note, the discussions above focus on “directly” quantifying  $^{235}\text{U}$  content with the  $^{235}\text{U}$  NRF response. The opportunity also exists for measuring the  $^{238}\text{U}$  content of the cylinder via the  $^{238}\text{U}$  NRF response, and using this metric as an “indirect” means of determining or constraining the net  $^{235}\text{U}$  mass. The potential advantage of interrogating the  $^{238}\text{U}$  content is that the specific NRF response (i.e. the response per unit mass) of  $^{238}\text{U}$  is roughly a factor of two larger than the  $^{235}\text{U}$  response, and the ratio of isotopic abundances,  $^{238}\text{U}/^{235}\text{U}$ , is in the range of 20:1 to 99:1 in typical LEU product. Thus, at a fixed background rate (which is independent of isotopic enrichment, as noted above), the signal-to-noise ratio for a  $^{238}\text{U}$  NRF metric can in principle be larger than that of the corresponding  $^{235}\text{U}$  metric by one to two orders of magnitude. These signal-rate considerations alone, however, do not necessarily imply a more precise enrichment measurement. For example, in a simple subtraction-based assay procedure in which the net  $^{235}\text{U}$  mass is determined from the total uranium mass in a  $\text{UF}_6$  cylinder, in conjunction with a calibrated  $^{238}\text{U}$  mass metric obtained via NRF, uncertainty in the  $^{238}\text{U}$  assay metric typically will dominate the uncertainty in the reconstructed  $^{235}\text{U}$  mass. The substantially larger  $^{238}\text{U}$  mass in a two-component LEU mix must, in fact, be determined to a precision of at least a factor of  $(\text{Mass}(^{238}\text{U})/\text{Mass}(^{235}\text{U}))$  better than the desired  $^{235}\text{U}$  assay relative uncertainty. Thus, although more signal would be available to exploit, the measurement precision requirements (and in turn the number of required counts,  $S_{\text{req}}$ ) would also be more stringent in this notional,  $^{238}\text{U}$ -based assay approach. It is desirable for the purposes of diversion detection to obtain positive (“direct”) confirmation of the  $^{235}\text{U}$  content in an inspected cylinder. Thus it is likely that any NRF-based assay protocol that makes use of the  $^{238}\text{U}$  response would be more complicated than this simple net-mass scheme, and would take both  $^{235}\text{U}$  and  $^{238}\text{U}$  signals into account in order to optimize the precision of the reconstructed enrichment. Dwell-time estimates for possible assay schemes incorporating the  $^{238}\text{U}$  response have not been made to date, in either scattering-mode or transmission-mode types of NRF measurement.

### III.C. Conclusions

This concept overview has summarized a measurement- and modeling-based feasibility assessment of NRF as a practical, active-interrogation assay method for  $\text{UF}_6$  cylinders at low product enrichment. This assessment, carried out under U.S. Department of Energy/NNSA funding, indicates that measurements in finite-angle scattering mode are not practical with currently-available gamma-ray detector technology and broad-spectrum bremsstrahlung photon beam sources. Requisite dwell times for a measurement of reasonable statistical precision (5% relative enrichment assay uncertainty) are on the order of several 10’s of hours. These dwell times are estimated on the basis of a DU measurement campaign in simplified slab-target geometry, extrapolated via measurement-validated NRF models of the  $^{235}\text{U}$  signal response to the  $\text{UF}_6$  cylinder-inspection scenario of interest.

NRF measurements in a simple “pass-through” transmission geometry, in which the path of the probe photon beam coincides with a diameter of the cylinder below the  $\text{UF}_6$  fill level, are similarly impractical due to photon attenuation. However, the feasibility of NRF measurements in a “grazing transmission” or “secant transmission” mode, with the interrogating photon beam incident along a secant of the cylinder and sampling a relatively limited portion of the  $\text{UF}_6$  contents, has not yet been quantitatively assessed. This measurement mode would offer an order of magnitude larger effective sampling path length than that probed in the traditional enrichment meter method, while leveraging the bulk mass of the  $\text{UF}_6$  itself as a shield against at least some portion of the photon background that limits system dead time in the finite-angle scattering



mode. Potential follow-on activities to the present UF<sub>6</sub> cylinder assay concept survey could involve a more thorough modeling-based assessment of various secant-path transmission mode NRF approaches, in tandem with bulk-target transmission mode NRF measurements to quantify typical signal-to-background ratios and target self-shielding effects. The potential utility of exploiting the <sup>238</sup>U NRF response in addition to the <sup>235</sup>U response should also be assessed.

### III.D. References

1. F.R. Metzger, "Resonance Fluorescence in Nuclei," Prog. Nucl. Phys. 7, 54-88 (1959).
2. U. Kniessl, H.H. Pitz and A. Zilges, "Investigation of Nuclear Structure by Resonance Fluorescence Scattering," Prog. Part. Nucl. Phys. 37, 349 (1996).
3. W. Bertozzi and R.J. Ledoux, "Nuclear resonance fluorescence imaging in nonintrusive cargo inspection," Nucl. Ins. Meth. Phys. Res. B 241, 820-825 (2005).
4. G.A. Warren, P.N. Peplowski, and R.S. Detwiler, *Nuclear Resonance Fluorescence Methods: FY2010 Annual Report*, Report no. PNNL-19987, Richland, Washington: Pacific Northwest National Laboratory (2010).
5. G.A. Warren, J.A. Caggiano, *FY08 Annual Report for Nuclear Resonance Fluorescence Imaging*, Report no. PNNL-18147, Richland, Washington: Pacific Northwest National Laboratory (2009).
6. W. Bertozzi et al., "Nuclear Resonance Fluorescence Excitations near 2 MeV in <sup>235</sup>U and <sup>239</sup>Pu," Physical Review C 78, 041601 (R) (2008).
7. G.A. Warren, P.N. Peplowski, and J.A. Caggiano. *NRF Methods: FY2009 Annual Report*, Report no. PNNL-19008, Richland, Washington: Pacific Northwest National Laboratory (2009).
8. D. Reilly, N. Ensslin, and H. Smith, Jr., *Passive Nondestructive Assay of Nuclear Materials*, Report no. NUREG/CR-5550, LA-UR-90-732, Los Alamos, New Mexico: Los Alamos National Laboratory (1991).

## IV. MEASUREMENTS OF CONTINUOUS-IN-ENERGY NEUTRON SOURCES USING THE BC-523A CAPTURE-GATED LIQUID SCINTILLATOR

*Marek Flaska, Sara Pozzi*  
*University of Michigan*

*James S. Bogard, Stephen S. Smith, Ana C. Raffo-Caiado*  
*Oak Ridge National Laboratory*

### IV.A. Introduction

Capture-gated organic scintillation detectors are promising for applications that require detailed neutron energy information, such as nuclear nonproliferation, international safeguards, and national security. In particular, for nuclear nonproliferation, fast and robust methods for the identification special nuclear material (SNM) are needed. The identification of SNM with capture-gated organic liquid scintillators using fast digital techniques is a very promising method and is based on the neutron spectroscopic information that is available from the detector.

The capture-gated detectors are based on standard organic scintillators that are loaded with material with high neutron absorption cross section. These materials are typically  $^{10}\text{B}$ ,  $^6\text{Li}$ , and  $^{\text{nat}}\text{Gd}$ . The capture-gated detectors have been studied extensively in the past [1-4]. The capture-gated neutron-spectroscopy principle is based on the fact that a single neutron creates two pulses that are related in time. The primary scattering neutron pulse from the scintillator is accepted only if a subsequent neutron capture pulse is detected. Also, the amplitude of the scattering can be used to estimate the incident neutron energy. The elapsed time between the neutron scattering pulse and the subsequent neutron capture is typically of the order of several hundreds of nanoseconds.

In this work, we present new experimental results obtained with the BC-523A detector, a boron-loaded (4.41 wt% of  $^{10}\text{B}$ ) liquid scintillator by Saint Gobain. The measurement results were compared to Monte Carlo simulations. The main objective of this work is to characterize the detector for several neutron energies to reveal the response of the detector. This information will be further used to design a new neutron-spectroscopy system based on the BC-523A detector.

### IV.B. Pulse Shape Discrimination for BC-523A

For standard liquid scintillators (BC-501A, EJ-309, etc.) an optimized offline digital PSD method is an excellent tool for distinguishing neutron pulses from gamma-ray pulses [5]. This method is based on the standard charge integration method which calculates the integral ratio of two different pulse intervals. Generally, the heavier the particle is, the larger fraction of light is in the tail of the pulse. This results in a larger ratio of tail-to-total-integrals for neutrons when compared to gamma rays. An identical PSD method was applied to the BC-523A detector.

In the initial measurements, a 1-Ci Pu-238–Be source was placed 30 cm from the face of the detector. To increase the relative number of measured neutrons, a 2-in. lead shielding block was placed between the source and the detector near the detector face. A 12-bit ADC250 waveform digitizer was used to collect several hundreds of thousand neutron and gamma-ray pulses. The digitizer operated at 250 MHz (4-ns sampling step) and each recorded waveform contained 60 steps (240 ns). The threshold was set to 30 keVee (keV electron equivalent).

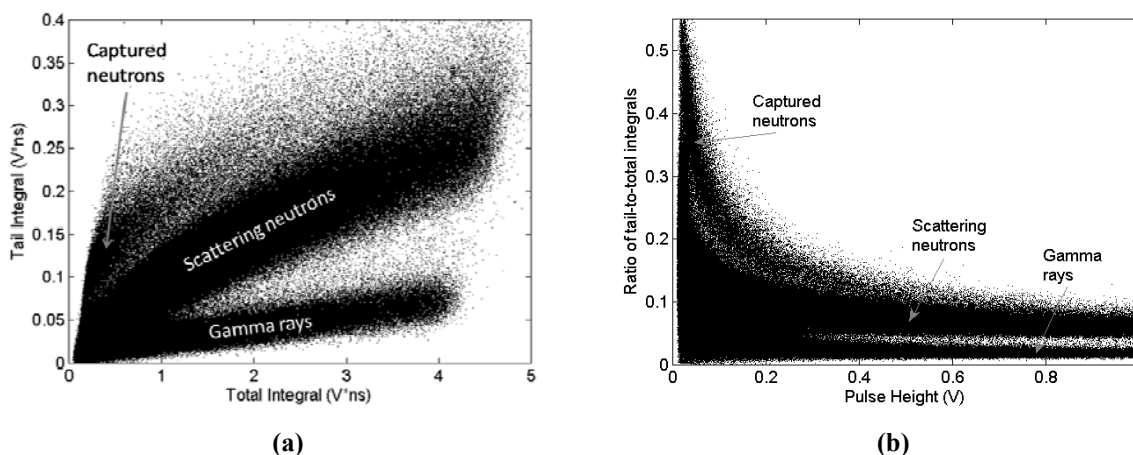


**Figure 1. (a) Tail integral versus total integral. Gamma-ray pulses can be distinguished not only from fast (scattering) neutron pulses, but also from thermal (capture) neutron pulses. (b) Ratio of tail-to-total integrals versus pulse height. Three regions of pulses are clearly distinguished.**

Figure 1 shows scattering and captured neutrons and scattering gamma rays. The neutron capture pulses and the neutron and gamma-ray scattering pulses measured with BC-523A are unambiguously identified by visual inspection. The identification is possible because the neutron capture reaction on B-10 generates a recoil alpha particle and a gamma ray, which generates a pulse that has a more pronounced tail than neutron and gamma-ray scattering pulses. This effect is shown in Figure 1(a), where the pulse tail integral is shown as a function of total integral, and in Figure 1(b), where the ratio of tail-to-total integrals is shown as a function of pulse height. There are a total of  $\sim 1.7 \times 10^6$  pulses shown in Figure 1. The capture pulses are observed at high ratio values, thus above the neutron and gamma-ray scattering pulses. A smaller number of pulses and smaller scales are shown in Figure 2 ( $\sim 6 \times 10^5$  pulses) to see the three regions more clearly. Approximately 1.6 % of the measured pulses are identified as capture pulses. The ratio of capture and neutron scattering pulses is approximately 2.3%.

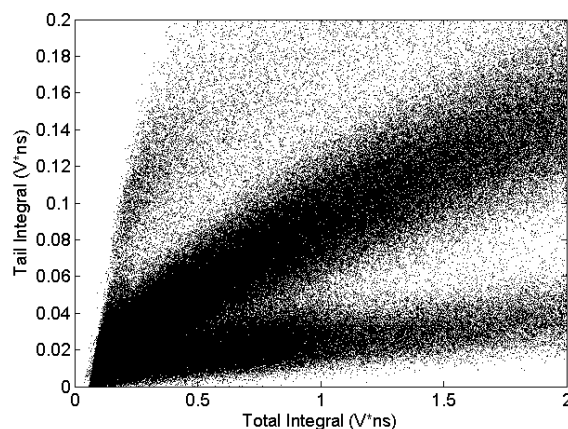


**Figure 2. Tail integral versus total integral. Good separation of captured neutrons from scattering neutrons and gamma rays is shown.**

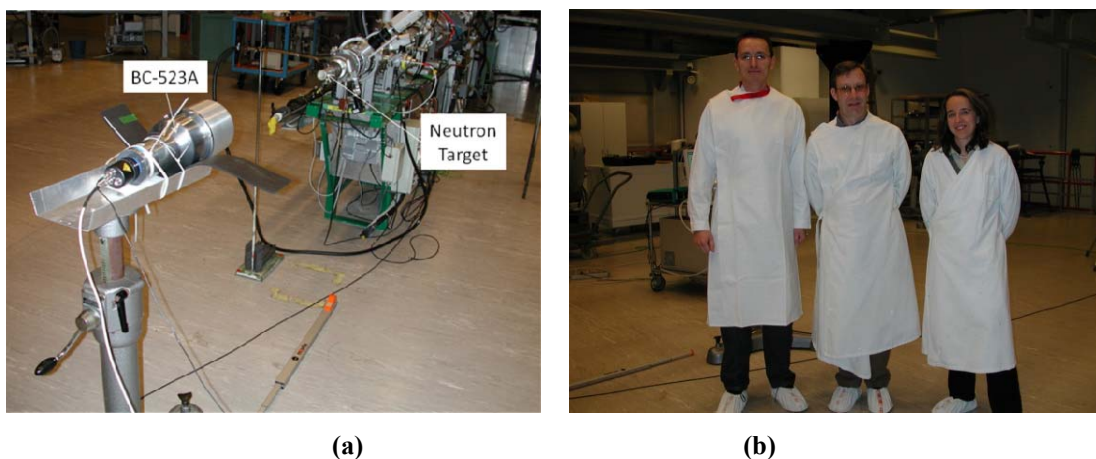
To verify the visual observation of three regions, the BC-523A detector was surrounded by 1 in. of polyethylene (PE). In addition, the Pu-Be source was placed inside a large borated PE storage barrel. One of the barrel ports was opened to allow the sources particles to reach the detector.

Again, the 2-in. Pb shielding was used between the open port of the source barrel and the detector. The PE shielding around the detector was used to increase the number of captured neutrons by backscattering the neutrons that would otherwise leave the detector. As expected, the number of captured neutrons increased by 12% in the presence of the PE when compared to the case without the PE. These results show that we have correctly identified the region of neutron capture pulses in results shown in Figure 1.

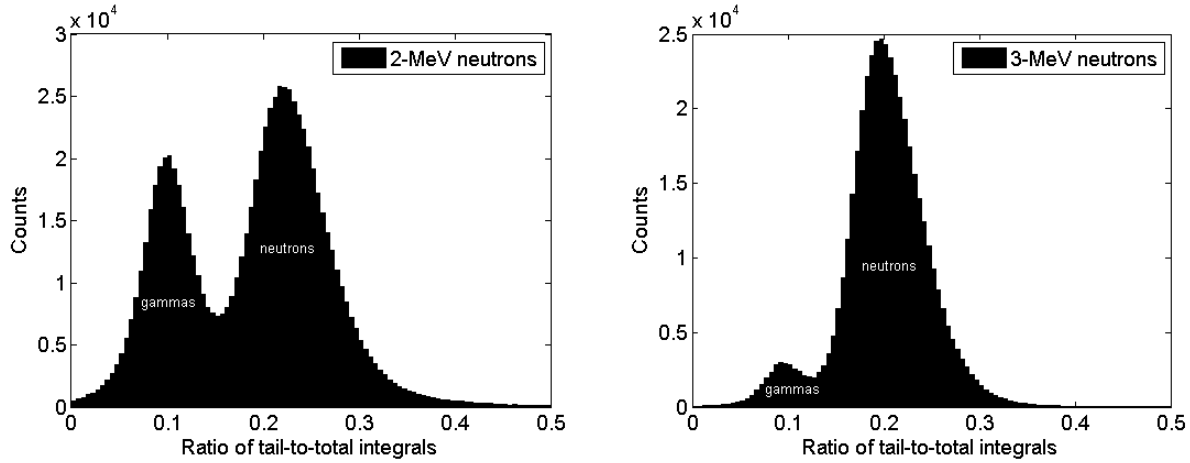
#### IV.C. Measurement and Simulation Results for Monoenergetic Neutrons

In the second measurement campaign, extensive calibration was performed at the Institute of Reference Materials and Measurements (IRMM) of the Joint Research Center (JRC) of the European Commission (EC). The EC-JRC-IRMM is located in Geel, Belgium and operates a 7 MV light-ion Van de Graaff accelerator. This facility was used to characterize the response of the detector for neutron energies between 800 keV and 6 MeV. The measurement setup and results are discussed below.

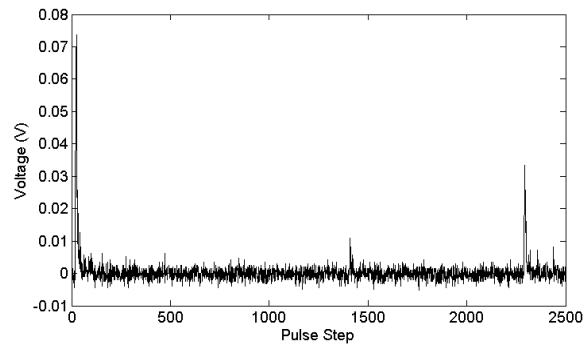
In the measurements, the detector was located approximately 1 m from a neutron-producing target, see Figure 3a. The research team is shown in Figure 3b. The targets that were used included LiF, tritium, and deuterium targets. Accelerated protons or deuterons were used in neutron producing reactions. A 10-bit, 4-channel Acqiris DC282 waveform digitizer was used to collect several hundreds of thousand neutron and gamma-ray pulses with relative number of gamma rays being different for each neutron energy. The number of gamma rays strongly depends on the type of neutron-producing target that is used and on the neutron energy; see Figure 4. The digitizer operated at 500 MHz (2-ns sampling step) and each recorded waveform contained 2500 steps (5  $\mu$ s data acquisition window). In contrast to the initial measurement, a long data-acquisition window was used to collect long waveforms containing primary and secondary neutron and gamma-ray pulses. Figure 5 shows an example of the waveform. The advantage of using a long data-acquisition window is the possibility of applying different thresholds to primary and secondary pulses. The disadvantage is a difficult ‘cleaning’ of the secondary pulses due to non-existing ‘point of reference’ in time.



**Figure 3. Photograph of the (a) detector in the target hall of the 7 MV Van de Graaff accelerator at EC-JRC-IRMM in Geel, Belgium, (b) research team. Small photo shows (from left) Cristian Mihailescu (digitizer operator) and Marek Flaska; large photo shows Marek Flaska, Goeran Loevestam (in charge with the Van de Graaff accelerator) and Sara Pozzi.**

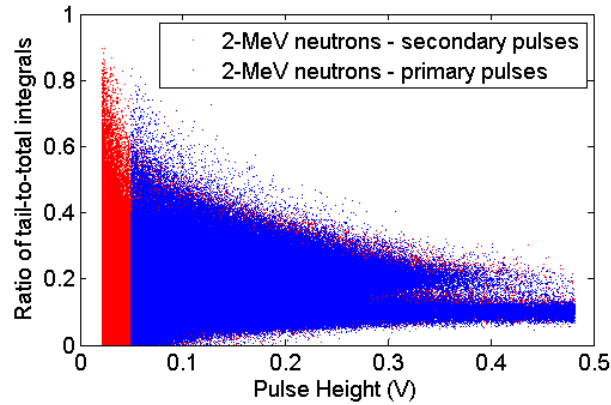


**Figure 4. Histograms of the primary pulses for 2 and 3 MeV neutrons. The pulses are sorted out based on their ratios of tail-to-total integrals. A large difference is observed between the relative numbers of neutrons in the 2 and 3 MeV measured data.**



**Figure 5. A waveform example acquired with the Acquiris DC282 digitizer. The waveform was measured with 1 MeV neutrons. The dynamic range of the digitizer was set to 0.5 V. Initially, the digitizer triggered on neutron (below 100 steps) and later a neutron capture pulse was recorded (~1400 steps). Before the end of the data acquisition window, another pulse was recorded, but it was discarded.**

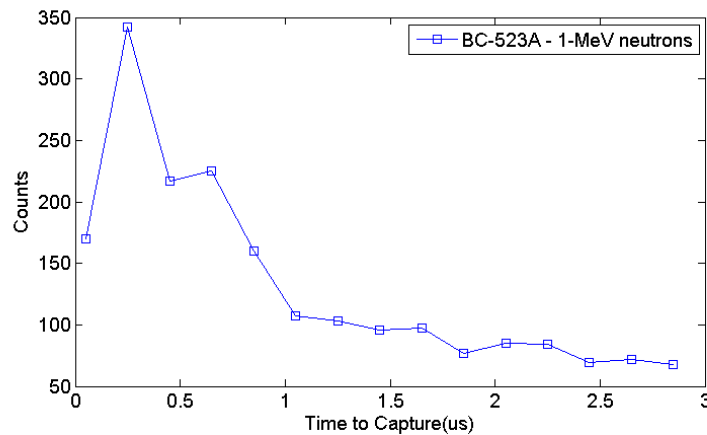
Because of the large range of the energies of interest three different digitizer ranges were used: 0.5, 1, and 2 V. The different range results in different effective resolution in the data sampling process, because the hardware resolution of the digitizer is constant. In addition, it results in different threshold for primary pulses because the digitizer has a minimum available threshold that depends on the dynamic range. Specifically, the measurement threshold for the 0.5 V range (800 keV, 1 MeV, and 2 MeV neutrons) was approximately 55 keVee, for the 1 V range (3 and 4 MeV neutrons) was approximately 110 keVee, and for the 2 V range (5 and 6 MeV neutrons) was approximately 220 keVee. For all measurements, the minimum available threshold was used. In the data post-processing part, the threshold for primary pulses was set to 70 keVee for 0.5 V range, while for the other ranges the original measurement thresholds were used. For the secondary pulses, the threshold was set to 30 keVee. This is illustrated in Figure 6 which shows ratios versus pulse heights for the 2 MeV case for both primary and secondary pulses.



**Figure 6. Histograms of the primary (in blue) and secondary (in red) pulses for 2 MeV measurements.**

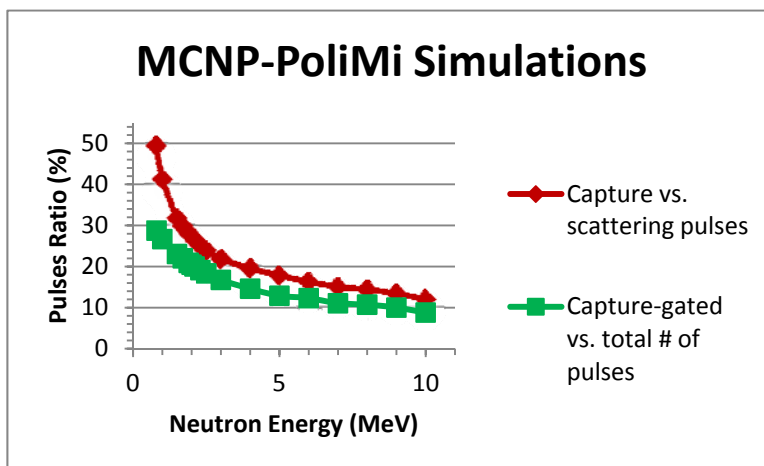
A special measurement data analysis algorithm was developed to obtain the information of interest from the measured. The algorithm works such that it first searches for primary pulses that are not distorted by signal(s) originating from other particle(s) colliding in the detector shortly after the initial particle. Next, the ‘clean’ primary pulse is classified as neutron or gamma ray based on its ratio of tail-to-total integrals. If it is classified as a neutron, the secondary pulse is searched for and its ratio of integrals is calculated. Finally, the secondary pulse is classified based on its ratio value and, if it is a capture pulse (large ratio values), the time that elapsed between this pulse and the primary neutron scattering pulse is calculated.

Figure 7 shows the time-to-capture distributions for the 1-MeV case. The expected mean time to capture for the detector is  $\sim 500$  ns [6]. The mean time values obtained from the measured time-to-capture distributions are approximately  $1 \mu\text{s}$  for 1- and 2-MeV cases, respectively. Similar values of approximately  $1.1 \mu\text{s}$  were obtained for energies between 3 and 6 MeV. These are less accurate values than previously published [7], which is probably caused by lower resolution of the digitizer and relatively low number of waveforms that were collected. The measured ratio of capture-gated neutron scattering pulses to the total number of pulses is approximately 0.7 and 0.4 % for 1 and 2 MeV neutrons, respectively. In Figure 7, 200 ns time binning was used. The initial increase in counts observed in Figure 7 is due to the width of the time window that is used for integration of pulses. This width is approximately 200 ns.



**Figure 7. Measured time-to-capture distribution for 1 MeV neutron beam. 200 ns binning was used. No errors are shown.**

In order to verify the measured results several Monte Carlo simulations were carried out. For these simulations, the MCNP-PoliMi code was used [8]. Figure 8 shows the simulated ratios of capture to scattering neutron pulses and capture-gated to total number of pulses, respectively. The simulations were performed for point isotropic sources placed in air and located 30 cm from the face of the BC-523A detector. The sources were simulated with energies between 0.8 and 10 MeV. For the scattering pulses, an 80 keVee threshold was used. Each time a capture event occurred in the detector model it was assumed that this event created a pulse that was detected with 100 % efficiency. Therefore, these simulated results are a conservative representation of measurement results that could be ideally obtained. Figure 8 shows that the relative number of captured neutrons strongly depends on the initial neutron energy. The capture to scattering ratio varies between 50 and 12 % while the paired to total ratio changes between 29 and 9 %.



**Figure 8. Simulated pulses ratios of interest. As expected, the relative number of captured neutrons, and consequently the number of capture-gated pulses, strongly depends on the initial neutron energy.**

Figure 9 shows various detection efficiencies simulated for the BC-523A detector. The total neutron detection efficiency (all neutron pulses included) starts at 53 % and decreases with increasing neutron energy. This is in agreement with the governing physics that takes place in the detector. The efficiency curve for scattered neutrons has peak at approximately 2 MeV; below this energy there are fewer scatterings (lower efficiency) expected because only a low number of elastic scatterings is needed before a neutron is captured. The capture-gated efficiency varies between 15 and 2.5 % and is similar to the efficiency for captured neutrons. These efficiencies are similar because most of the neutron capture events are preceded by neutron elastic scattering(s). The reader can see that the simulated capture-gated efficiency for 1 MeV neutrons is larger than the measured one (14 % versus 0.5 %). This effect is mainly caused by ideal treatment of captured neutrons and consequent creation of pulses in the simulations. In the future, our simulation tools will be improved to treat capture pulses more realistically. It is also expected that this difference in efficiency is caused by relatively large uncertainty of the measured value.



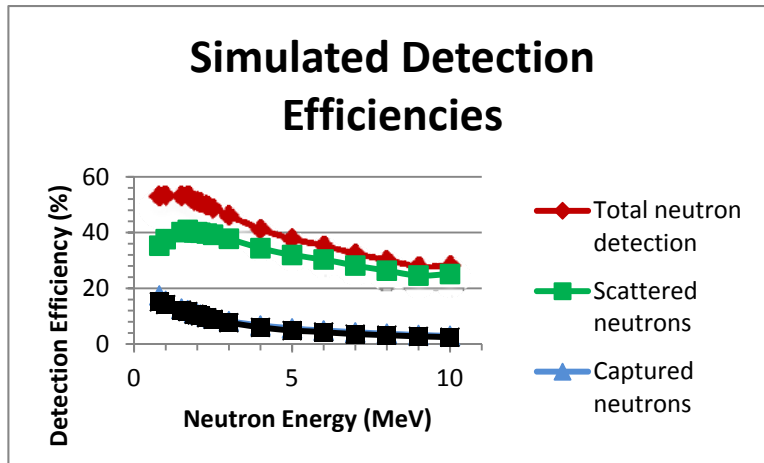


Fig. 9. Neutron detection efficiencies simulated with MCNP-PoliMi for the BC-523A detector.

#### IV.D. Measurement Results for Various Neutron Sources

A third measurement campaign took place at ORNL in August 2009. The following sources were used: Pu-238/Be, Pu-239/Be, Am/Be, Am/Li (alpha-n sources), and Cf-252 (spontaneous-fission source). Figure 10 shows the sources and the detector used in the measurements. The measurement source-detector distances were 56, 113, 154, and 15 cm for the Pu-239/Be, Am/Be, Pu-238/Be, and Am/Li, respectively. In the case of the Cf-252, the source-detector distance was set to 8.2 m to minimize the measurement count rate. Figure 11 shows the installation of a 4-in. lead shielding in front of and around the detector. In the case of the Am/Li source, 0.5 in. of lead was used as a shielding of the face of the detector. For all the other sources, 2 in. of lead was used in front of the detector.

Eight-channel, 12-bit, 250-MHz, CAEN V1720 waveform digitizer was used to sample signal from the detector and store time and signal data. The sampling step is 4 ns which gives 76 points per each measured pulse with the total data acquisition window of 304 ns. This time represents the system dead time, because any waveform containing a double peak (another potential pulse) is deleted to allow for data integration required for pulse shape discrimination (PSD).

A fixed measurement threshold of 50 keVee (50 keV electron equivalent) was used in all measurements. This light output value corresponds to approximately 330 keV neutron energy deposited. An optimized, offline PSD technique based on analog charge integration was utilized to separate capture pulses from scattering pulses and neutrons from gamma rays.

For standard liquid scintillators we frequently use an optimized offline digital PSD method [5]. This method is based on the standard charge integration method which calculates the ratio of two different pulse intervals. Generally, the heavier the particle is the larger fraction of light is in the tail of the pulse (larger tail integral in fixed integration range). This scintillator property results in a larger integration ratio when compared to gamma rays. This PSD method was applied to the BC-523A detector. The particle discrimination was performed offline, although the same method can be applied online by using a fast digitizer. This online possibility is promising for future detection systems based on capture-gated detectors. Figure 11a shows the description of the particle discrimination technique. Figure 11b shows a typical performance of the PSD technique for an EJ-309 liquid scintillator.



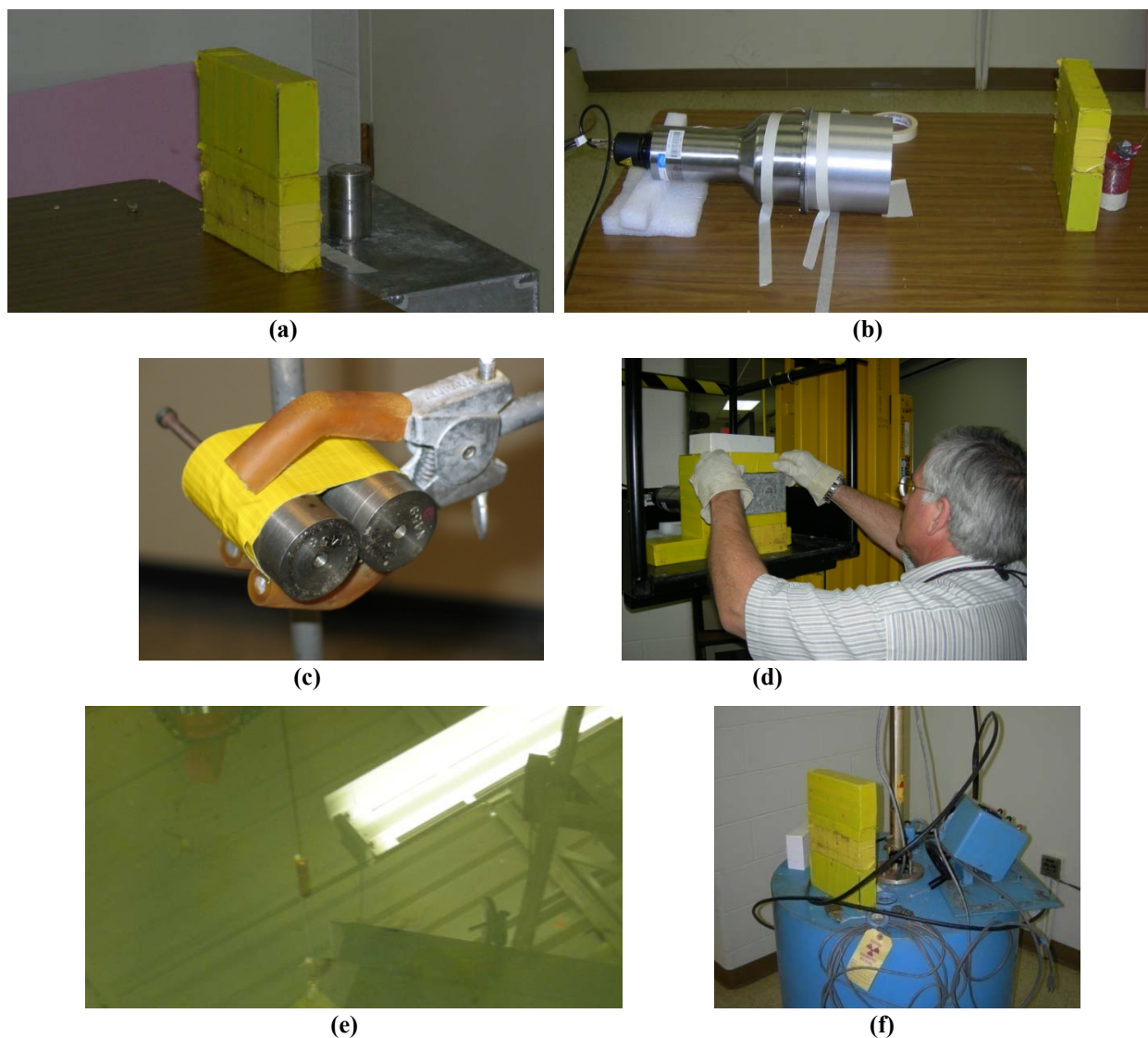


**Figure 10. (a) ~1-Ci Pu-238/Be source, (b) ~5-Ci Am/Be source, (c) ~8.5-Ci Pu-238/Be, (d) 1.5e9 neutrons/s Cf-252 source, and (e) ~2-Ci Am/Li source. The sources were placed at different distances from the BC-523A detector to obtain a measurement count rate of approximately 9,000 counts/s for the alpha-n sources (~2,000 counts/s for Am/Li). In the case of the Cf-252, the count rate was approximately 25,000 counts/s. (d) The Cf-252 source is shown in the storage pool. (f) Installation of lead shielding around the BC-523A detector for the Cf-252 measurement.**

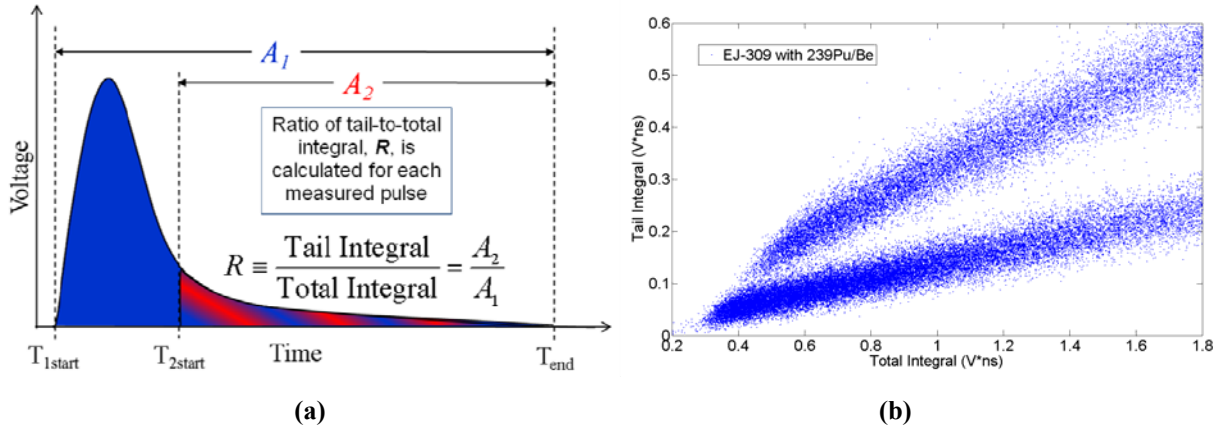


**Figure 11. (a) Description of a standard charge integration technique. Particles are discriminated based on their ratios of tail and total integrals. Generally, neutron pulses provide larger ratio values than gamma-ray pulses, which is caused by the amount of ‘delayed’ light from protons when compared to electrons. (b) Tail versus total integral for an EJ-309 liquid scintillation detector. A Pu-239/Be source was used at a threshold of 80 keVee (~ 500 keV neutron energy deposited). Each point represents one pulse. Excellent separation of neutrons (top region) from gamma rays (bottom region) is observed.**

#### IV.E. Pulse Shape Discrimination for BC-523A

Three pulse regions are observed in the data obtained with the BC-523A, see Figure 12. In addition to neutron and gamma-ray scattering pulses seen in Figure 11b, a third region of neutron capture pulses is observed. These capture pulses are used to ‘confirm’ neutron scattering pulses. The particle discrimination become slightly worse compared to EJ-309 due to different chemical/light properties of the BC-523A liquid. Average time between initial neutron scattering pulse and consequent capture pulse claimed by the manufacturer is approximately 450 ns for the BC-523A detector. The number of captured neutrons decreases exponentially with time, which means that the size of a single data acquisition window must be chosen as narrow as possible to maximize the number of measured capture pulses (minimize the dead time of the system). The other data-acquisition option is to use a waveform window that is long enough to cover the time region of interest. In that case, both primary and secondary pulses are contained in a single waveform.

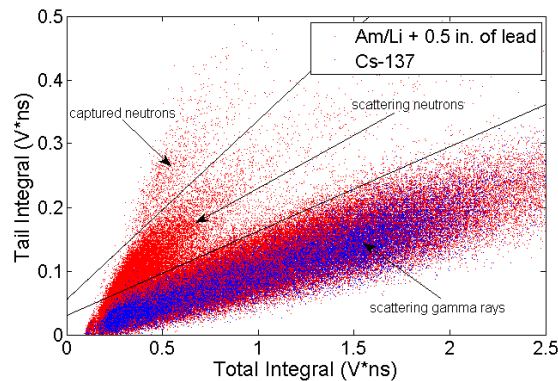


**Figure 12. Tail vs. total integral for the Am/Li source shielded with 0.5 in. of lead. Three regions of pulses are observed: captured neutrons, scattering neutrons, and scattering gamma rays.**

The PSD was optimized to maximize the separation of the three regions of interest. Figure 13 shows how the starting point of the tail integral changes the separation of the regions.

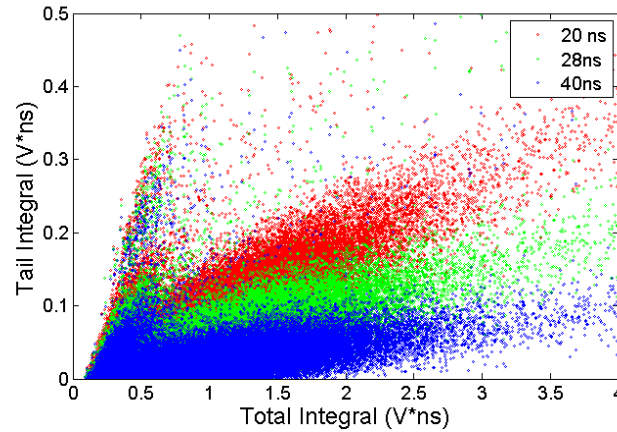


**Figure 13. Tail vs. total integral for the bare Am/Li source. The end point for both PSD integrals was set to 224 ns from the pulse maximum, while the start point of the tail integral varied between 20 (in red) and 40 ns (in blue) from the pulse maximum. 20-ns option was chosen for the investigation.**

#### IV.F. Measurement Results and Analysis

Neutron scattering pulses were capture-gated by using the neutron capture pulses. Figure 14 shows the obtained neutron pulse height distributions for four different sources. As expected, the Cf-252 distribution has lower values at high light output values due to lower average neutron energy of the source spectrum (essentially Watt spectrum; 2.1-MeV average energy) when compared to the alpha-n sources Pu-238/Be, Pu-239/Be, and Am/Be. No significant differences are observed among the alpha-n sources because of their similar average neutron energy (approximately 4.5 MeV). As observed in the past, a spontaneous-fission neutron source can be visually differentiated from an alpha-n neutron source when measured with a BC-501A liquid scintillator [5]. This result indicates that the offline data-postprocessing algorithm was correctly optimized because similar results were obtained when compared to BC-501A (BC-523A is based on BC-501A).

The distributions shown in Figure 14 can be unfolded to obtain the initial source neutron spectra. However, the unfolding process requires detailed knowledge of energy-dependent light outputs for the detector. This so-called response matrix has to be accurately measured or simulated; each of these approaches has its advantages and disadvantages. Moreover, the unfolding can be also used for standard liquid scintillators so this cannot be used to justify the use of the BC-523A capture-gated detector instead of a liquid scintillator such as EJ-309. The obvious disadvantage of using the BC-523A instead of EJ-309 is its lower efficiency as a result of the gating process [6]. On the other hand, the main advantage is that the BC-523A provides information about how many neutrons were captured in the BC-523A. The number of captured neutrons relative to the number of scattering neutrons is influenced by the capture probability, which changes with the energy of the incident neutrons. Thus, the ratio of measured neutron capture pulses and scattering pulses is related to the average energy of the incoming neutrons, a property that can be used for material identification. In such case, the detector time response is significantly shortened because no pulse height distributions (good statistics is needed) have to be acquired. The detector response for obtaining the neutron pulse height distributions is of the order of minutes,

depending on the neutron intensity. This crude approach might prove useful for identification of neutron-emitting material when very fast detector response is required. Table 1 shows the number of measured pulses and the average pulse heights for each measurement.

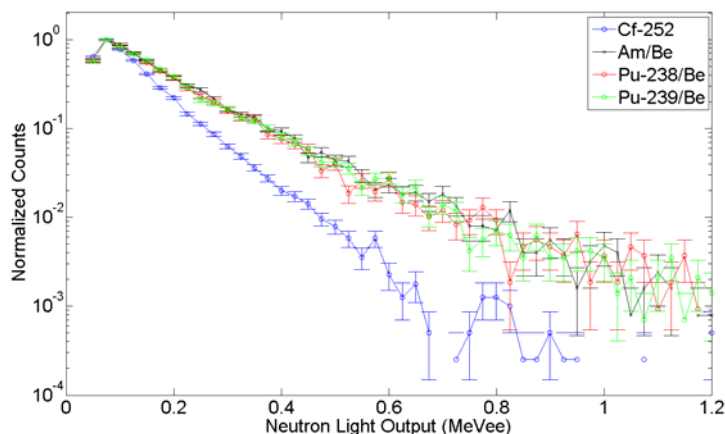


Figure 14. Neutron pulse height distributions for various neutron sources. Square-root errors are shown. The  $^{252}\text{Cf}$  distribution has lower values at high light output values due to lower average neutron energy of the source spectrum when compared to alpha-n sources. As expected, no significant differences are observed among the alpha-n sources. The Am-Li result is not shown; the Am-Li pulse height distribution can be easily distinguished from the other distributions due to its very low neutron-energy average ( $\sim 400$  keV).

Table 1. Summary of the measurement results. “ph” stands for pulse height.

Source type	Pu-239/Be with 2 in. of lead	Am/Be with 2 in. of lead	Pu-238/Be with 2 in. of lead	Cf-252 with 4 in. of lead
Size of the gating window (us)	10	10	10	10
# of scattering gammas (%)	42.38	54.16	58.76	71.42
# of scattering neutrons (%)	55.26	44.23	39.73	26.87
# of captured neutrons (%)	2.36	1.61	1.51	1.71
# of capture-gated neutrons (%)	0.22	0.16	0.13	0.33
# of captured neutrons relative to scattering neutrons (%)	4.27	3.64	3.80	6.36
Total # of pulses	12,455,607	18,959,713	19,845,103	13,578,631
Average ph for scattering gammas (keVee)	281	252	265	207
Average ph for scattering neutrons (keVee)	429	423	409	253
Average ph for captured neutrons (keVee)	154	160	151	120
Average ph for capture-gated neutrons (keVee)	506	532	510	259

For all data analysis, the size of the time capture-gated window was set to 10  $\mu$ s. The Am/Li results are not shown in Table 1 due to low counting statistics of the data (intrinsically very low number of neutrons relative to the total number of particles emitted from an Am/Li source). It should be noted that the BC-523A detector had to be placed at a large distance from the Cf-252 because of the strength of the source. Also, a large amount of shielding had to be used in front of (a factor of two more compared to other sources) and around the detector to reduce the detection count rate.

Some interesting comparisons can be made among the values shown in Table 1. First, the ratio of capture-to-scattering neutrons is approximately 4 for the alpha-n sources, while for the Cf-252 it is more than 6. This is because neutrons with lower incident energies have higher probability of being captured after they have deposited most of their energy in the detector by scatterings. As already mentioned above, the capture-to-scattering ratio can be measured significantly faster than the actual capture-gated-neutron pulse height distribution, which means the identification of the material under investigation can also be done faster. Although the difference in the lead shielding has some effect on the ratio values described above it is caused mainly by the incident-energy difference.

Second, the measured average neutron and gamma-ray pulse heights can be used to complement the ratio values to make them more reliable. For example, the average pulse height for scattering neutrons is significantly larger for the alpha-n sources ( $\sim 420$  keVee) than for the Cf-252 ( $\sim 250$  keVee). This indicates two possibilities: lower neutron energies and/or neutron shielding is present that moderates neutrons to lower energies. This information can be combined, to utilize the dual particle sensitivity, with the information on the measured average pulse height for scattering gamma-ray pulses to find out more about the measured material. For illustration, measured pulse height distributions for the Pu-238/Be source are shown in Figure 15. Such results can be obtained by post-processing the measured data if complete pulse height distributions are needed for unfolding.

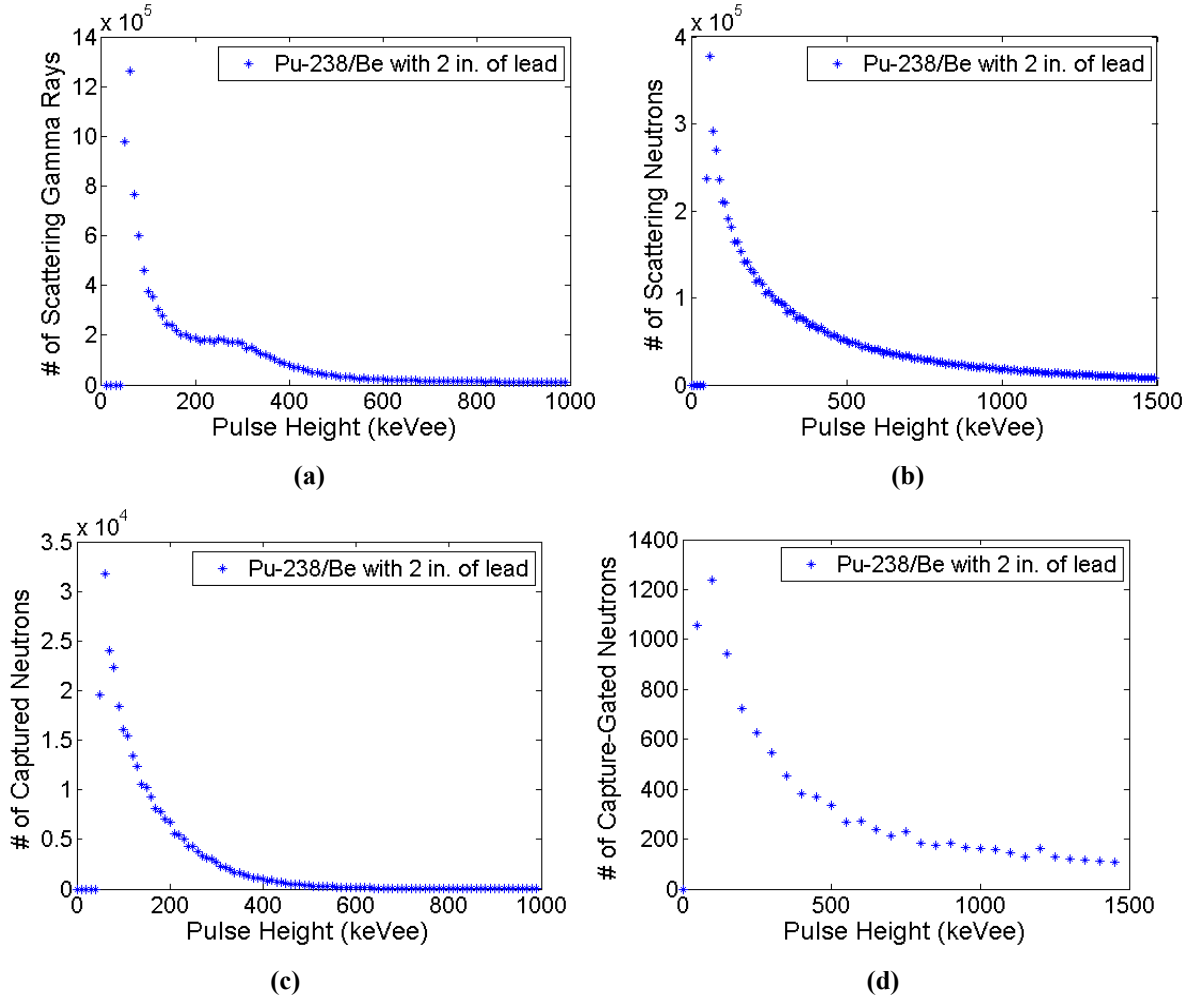


**Figure 15. Measured pulse height distribution for (a) scattering gamma rays, (b) scattering neutrons, (c) captured neutrons, and (d) capture-gated neutrons. The distributions were measured with the BC-523A and the Pu-238/Be shielded with 2 in. of lead.**

#### IV.G. Conclusions

Numerous measurements were performed with the BC-523A detector to determine the detector's potential for capture-gated neutron spectroscopy. It has been shown that captured neutrons can be distinguished from scattering neutrons and gamma rays by digital pulse shape analysis.

The BC-523A detector is less prone to neutron misclassification due to the presence of the additional neutron signal when compared to standard liquid scintillators (such as EJ-309). Although the neutron (capture-gated) sensitivity of the BC-523A is much lower than the neutron sensitivity of the EJ-309, the number of capture pulses can be used to estimate the energy of incoming neutron for material identification. It was shown that the spectroscopic information obtained from the detector can be used to discriminate the ( $\alpha$ , n) sources Pu-238/Be, Pu-239/Be, and Am/Be from the Cf-252 source and the Am/Li source by using measured quantities such as ratios of the number of captured neutrons to scattering neutrons. This discrimination can be performed without having to acquire complete neutron pulse height distributions. This technique has the potential of reducing measurement times needed for accurate discrimination of the sources (with fully optimized detection system and detector size) when compared to the

standard organic scintillators. Therefore, the BC-523A detector could be utilized in the area of the characterization of special nuclear material but also of neutron sources in general because these detectors can be built reasonably small for hand-held devices, while still being efficient. In fact, detection systems based on the measurement of both neutrons and gamma rays are less prone to false alarms, especially in the presence of shielding. BC-523A operates at room temperature. System response is expected to be of the order of minutes, depending on the source intensity. The BC-523A detector could be used to measure UF<sub>6</sub> cylinders, but tests are still to be conducted in this field. Since the detector can measure both gammas and neutrons, one could analyze the 186 keV gamma and the alpha-n neutrons at the same time.

#### IV.H. References

1. D.M. Drake, W.C. Feldman, C. Hurlbut, *Nucl. Instr. and Meth. A* 247 (1986) 576.
2. H.P. Chou, C.Y. Horng, *Nucl. Instr. and Meth. A* 328 (1993) 522.
3. B. Czirr, G. Jensen, *Nucl. Instr. and Meth. A* 349 (1994) 532.
4. B. Czirr, D. Merrill, D. Buehler, *Nucl. Instr. and Meth. A* 476 (2002) 309.
5. M. Flaska, S.A. Pozzi, *Nucl. Instr. and Meth. A* 577 (2007) 654.
6. M. Flaska, S.A. Pozzi, *Nucl. Instr. and Meth. A* 599 (2009) 221.
7. S.A. Pozzi, E. Padovani, M. Marseguerra, *Nucl. Instr. and Meth. A* 513 (2003) 550.

## V. ASSESSMENT OF ELPASOLITE SCINTILLATORS WITH NEUTRON/GAMMA DISCRIMINATION AS THE BASIS FOR A HYBRID PASSIVE ENRICHMENT METER SYSTEM

*Benjamin S. McDonald, Mitchell Myjak, Christopher R. Orton, Emily Mace, David Jordan  
Pacific Northwest National Laboratory*

### V.A. Introduction

Neutron-sensitive, medium gamma-ray energy resolution Elpasolite scintillators (e.g., CLYC [1]) are recently commercially available and are being evaluated for several radiation detection scenarios at PNNL. Assaying  $\text{UF}_6$  enrichment may be a good application area for such detectors. A CLYC-based unattended monitoring system of  $\text{UF}_6$  cylinders could combine the capabilities of two other currently-developed systems, the Hybrid Enrichment Verification Assay (HEVA) from Pacific Northwest National Laboratory [2] and the Passive Neutron Enrichment Meter (PNEM) from Los Alamos National Laboratory [3].

### V.B. Combining Passive Enrichment Techniques

PNNL is developing the hybrid enrichment verification array (HEVA) method, which utilizes high-energy gamma-ray signatures created by penetrating neutron emissions from  $\text{UF}_6$  [2]. This method only requires NaI gamma-ray detectors, but could be enhanced to include techniques developed for the LANL PNEM system [3] by using neutron-sensitive scintillators instead of NaI. In addition to  $^{235}\text{U}$  wt %, the PNEM system is able to estimate the uranium mass, the  $^{234}\text{U}$  mass, and the multiplication. Combining the HEVA and PNEM methods with a CLYC-based detector system could measure enrichment in multiple, corroborating ways for less cost than He-3 based systems. With CLYC detectors gammas and neutrons can be discriminated based on pulse height or pulse shape data. Energetic charged reaction products from thermal neutron capture on  $^6\text{Li}$  generate scintillation pulses near 3.1 MeV electron-equivalent (MeVee). Measurements with a variety of gamma-ray sources and a  $^{252}\text{Cf}$  neutron source (Figure 1) suggest that pulse-shape analysis is not necessarily needed to exploit the CLYC neutron information; the distribution in pulse-height cleanly distinguishes the neutron response. In HEVA, the non-traditional metric (NaI detector photopeak and continuum response to neutron-induced high-energy gamma rays) is the sum of counts from 3-8.5 MeV. Directly-detected neutrons in a CLYC detector would add signal to the indirect HEVA NaI detector data.

Multiple neutron-induced assay metrics, including those derived from CLYC detector high-energy responses and PNEM data, could be combined in a variety of ways. Separate  $^{235}\text{U}$  mass calibrations can be performed for the various signal types separately, and the assay results derived from the separate calibrations averaged (with appropriate weighting to reflect differences in measurement precision based upon counting statistics). Alternatively, a summed-response metric involving the various signal types (again with error-weighting for the contributing responses) can be adopted for the calibration process and subsequent assay.



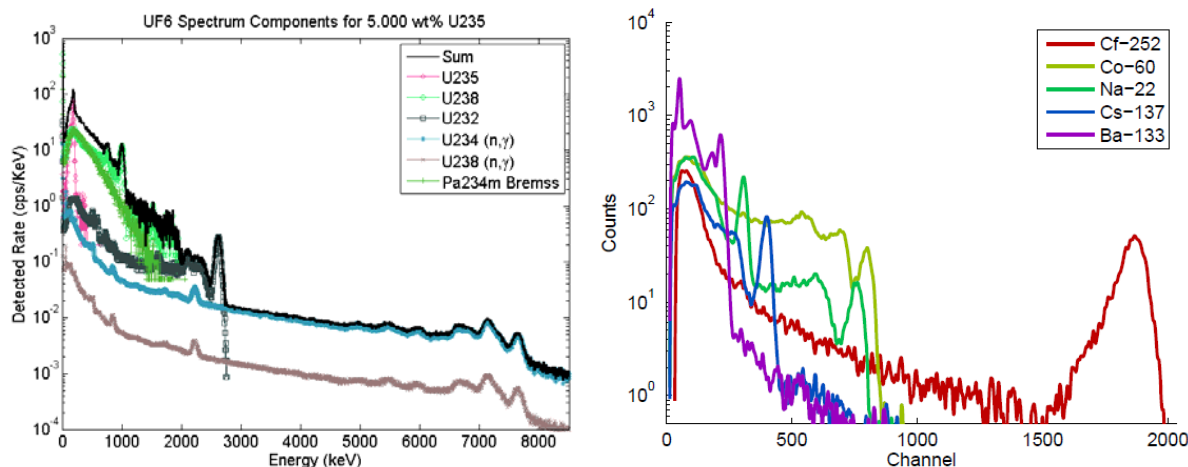


**Figure 1. Left panel: Simulated isotopic spectral components from  $\text{UF}_6$  as detected by a 3x3 NaI detector in HEVA. Right panel: Measured spectra in a 1" CLYC detector. The neutron-induced signals in both detectors have very little interference or background from other sources.**

### V.C. Conclusions

A variety of neutron-induced assay metrics are available for characterizing  $^{235}\text{U}$  content of  $\text{UF}_6$  cylinders. The neutron-sensitive inorganic scintillator, CLYC, offers a complementary detection approach to those under current investigation in the HEVA and PNEM systems. Combining the neutron-response metrics from the various approaches may yield greater assay precision and/or robustness against systematic assay uncertainties.

### V.D. References

1. J. Glodo, K. Shah, U. Shirwadkar, S. Mukhoopadhyay, R. Hawrami, C. Hines, A. Churilov, W. Higgins, J. Tower, P. O'Dougherty, H. Hong, T. Hazlett, "CLYC Scintillators," *Neutron Detection Technologies Workshop*, IAEA, (2011).
2. B. S. McDonald, Jordan, D.V., Orton, C.T., Mace, E.K., Wittman, R.S., Smith, L.E., "Model and Algorithm Evaluation for the Hybrid  $\text{UF}_6$  Container Inspection System," *Institute of Nuclear Materials Management Annual Meeting*, (2011).
3. K. A. Miller, H. O. Menlove, M. T. Swinhoe, and J. B. Marlow, "A New Technique for Uranium Cylinder Assay Using Passive Neutron Self-Interrogation," in IAEA Symposium on International Safeguards, Vienna, Austria, (2010).

## VI. USE OF SPECIFIC THICK TARGET ALPHA PARTICLE INDUCED REACTION GAMMA RAY YIELDS FOR VARIOUS NUCLIDES IN URANIUM HEXAFLUORIDE AS A WAY TO ESTIMATE $^{234}\text{U}$ ABUNDANCE

*Stephen Croft, Martyn T. Swinhoe, Karen A. Miller  
Los Alamos National Laboratory*

### VI.A. Abstract

Fluorine has a relatively large ( $\alpha, n$ ) production cross section in the MeV range, the range of interest for special nuclear materials. Enriched  $\text{UF}_6$  in particular is a reasonably prolific source of ( $\alpha, n$ ) neutrons because along with  $^{235}\text{U}$ ,  $^{234}\text{U}$  becomes enriched and it has a relatively short half-life. This enables storage cylinders containing  $\text{UF}_6$  to be verified by neutron counting methods.

In association with such measurements high resolution gamma ray spectrometry measurements using a high-purity Ge detector are often undertaken to determine the enrichment based off the intensity of the direct 186 keV line. The specific ( $\alpha, n$ ) neutron production, neutrons per second per gram of U, is sensitive to the relative isotopic composition, particularly the  $^{234}\text{U}$  concentration, and in the traditional gross neutron counting approach is needed to quantitatively interpret the data.

In addition to  $\text{F}(\alpha, n)$  neutrons,  $\alpha$ -induced reaction gamma rays are generated, notably at 110, 197, 582, 891, 1,236 and 1,275 keV. If one could observe  $^{19}\text{F}(\alpha, x\gamma)$  gamma lines in the HRGS spectra the thought was that perhaps the  $\alpha$ -activity could be estimated directly, and in turn the  $^{234}\text{U}$  abundance obtained. For example, by utilizing the ratio of the detected 197 keV to 186 keV full energy peaks. However, until now there has been no readily available estimate of the expected strength of the reaction gamma-rays nor any serious consideration as to whether they might be diagnostic or not.

In this work we compute the thick target yields of the chief reaction gamma rays in  $\text{UF}_6$  using published thin target data. Comparisons are made to the neutron production rates to obtain  $\gamma/n$  estimates, and also to the  $^{235}\text{U}$  decay line at 186 keV which we take as a fiducial line. It is shown that the reaction gamma rays are produced but are far too weak for practical purposes.

Now that the underlying numerical data is readily available however, it can be used to support calculations in other fluorine compounds, for example impure plutonium reference materials where fluorine may be present only at the ppm level yet still present a serious nuisance addition to the neutron production rate.

### VI.B. Introduction

Concerns over mankind's potential influence on the Earth's climate coupled with global energy supply worries have recently rekindled interest in the expansion nuclear power. The growth of nuclear power requires a new generation of nuclear facilities including large capacity gas centrifuge enrichment plants (GCEPs). Attention has therefore fallen onto how advanced technologies can be applied to effectively safeguard the  $\text{UF}_6$  arriving at, maintained in, and leaving such facilities. This is motivated in part by the need to verify by best practical means, given the realities of finite resources, that States are in compliance with their obligations under international agreements.

The majority of  $\text{UF}_6$  at GCEPs is contained in storage cylinders because the in-process inventory is comparatively small. Feed and tails are typically held in 48" diameter cylinders and product in 30" diameter cylinders. Thus methods to independently assay bulk  $\text{UF}_6$  have received particular attention. The high penetrability of the fission and  $(\alpha, n)$  neutrons produced by  $\text{UF}_6$  exploited in combination with a relative isotopic composition determination has been an attractive traditional approach achieving a pragmatic nondestructive solution for the verification of such items. A basic gamma-ray measurement based on the enrichment meter principle [1] provides the enrichment value. From this the specific neutron source term, which is dominated by  $^{234}\text{U}(\alpha, n)$  and  $^{238}\text{U}$  spontaneous fission neutrons, can be inferred. The net observed neutron counting rate emerging from the cylinder in a calibrated configuration is then used to verify the bulk amount of  $\text{UF}_6$  present [2]. One weakness of this approach is that the  $^{234}\text{U}$  abundance is not directly measured but must be inferred from an assumed correlation with enrichment. The  $^{234}\text{U}$  fraction cannot be measured by the usual isotopic gamma spectral analysis methods through the thick container walls. Several possibilities to overcome this concern suggest themselves. One approach in development is to acquire coincidence count data in addition to the gross signal and use it in combination to determine the fissile content from the strength of the self-induced fission rate [3]. Another concept under consideration is to use reflected neutrons to interrogate the material together with temporal discrimination [4].

The question we pose here is whether there is a signature in the high-resolution gamma-ray spectrum which can be used to quantify the  $^{234}\text{U}$ -to- $^{235}\text{U}$  ratio. Specifically we evaluate the strength of the  $(\alpha, x\gamma)$   $\alpha$ -induced reaction gamma rays. Those lines close in energy to the 186 keV line resulting from the decay of  $^{235}\text{U}$  could be ratioed with it without requiring a large transmission correction while those of higher energy might offer a benefit by being more penetrating.

### VI.C. Background

The  $^{19}\text{F}(\alpha, n)^{22}\text{Na}$  reaction has a Q value of about -1.92MeV. For  $^{234}\text{U}$   $\alpha$ -particles this means that the residual  $^{22}\text{Na}$  nucleus maybe excited up to about 1.98MeV. Including the ground states this means there should be 8 levels energetically open. In keV these are, along with spin assignments: 1,983(3+), 1,952(2+), 1,937(1+), 1,528(5+), 891(4+), 657(0+), 583(1+) and 0(3+).

Neutrons with energies up to about 2.5MeV are to be expected. According to basic statistical nuclear theory the mean energy will be circa 1.1MeV for  $^{234}\text{U}$   $\alpha$ -particles. The neutron strength at either extreme of the allowed energy distribution is expected to fall to zero. The highest energy neutrons correspond to the  $^{22}\text{Na}$  nucleus being left in the lower levels (gs up) while the soft end of the neutron spectrum will leave the nucleus highly excited. The 1,983-, 1,952- and 1,937-keV levels feed the 891-keV level but only weakly. The 891-keV level can also be created directly although perhaps not dominantly. From the level diagram the 583-keV line should be present and reasonably strong.

Based on this initial survey of reaction channels [5] one might conclude that the strength of the reaction gamma rays ought to be comparable to that of the neutron strength. In the case of plutonium compounds we also know this to be the case [6] and reaction gamma lines from fluorine are used to flag the presence of this element in plutonium contaminated waste, a clear indication that the  $(\alpha, n)$  to spontaneous fission neutron yield may be high compared to metal or oxide, for example. It is tempting therefore to ask whether the  $\alpha$ -induced reaction gamma-rays from  $\text{UF}_6$  might be observed and used to support international safeguards verification efforts.

## VI.D. Method

There is strong evidence that the  $F(\alpha, n)$  yield data contains large uncertainties [7-9], far larger than claimed by the experimenters contributing to the pool of results available for evaluation and far larger than is reasonable to expect from the proper application of the well established neutron metrology techniques applied to the problem. Having said this, for our present needs the work of Croft [7] serves as a convenient and justifiable reference source for thick target specific  $(\alpha, n)$  neutron yield data in  $UF_6$  and other compounds. We shall see later that for our feasibility assessment great accuracy is not needed. Although data for many  $\alpha$ -emitting nuclides are listed for our present discussion we are only concerned with the three naturally occurring isotopes of uranium,  $^{234}, ^{235}, ^{238}U$ .

In addition to  $(\alpha, n)$  neutrons low-enriched  $UF_6$  is also a source of spontaneous fission neutrons. This contribution may be estimated from known spontaneous fission half-life data taken in conjunction with the measured or estimated mean number of prompt neutrons liberated per fission and a predicted (based on nuclear systematic) estimate of the average number of delayed neutrons emitted from the remnants. In the present work we used an updated version of [12]. Again we shall see that exact values are not needed for our present purposes.

Corresponding data for gamma ray production is not available. To generate the necessary data we extracted elemental integrated over angle production gamma cross sections for fluorine from the plots reported in [10]. These are based on measurements made using a thin NaF target at an accelerator facility as a function of energy. Details on how the data collected was reduced to microscopic cross sections is not given in [10]. Corresponding thick target yields as a function of energy for  $UF_6$  were then calculated over the energy range 3.8 MeV to 10 MeV according to the continuous slowing down model outlined in [7]. For this step mass stopping power data was mixed according to the Bragg-Kleeman additivity rule using NIST's ASTAR evaluated physical data library [11]. An energy increment of 0.1 MeV was used. The yield curves were entered into a bespoke code which overlays the  $\alpha$ -line spectrum from a library of nuclide to give specific yield data,  $\gamma/\text{sec/gram}$ . This is the same code as was used to generate the specific  $UF_6(\alpha, n)$  yields.

## VI.E. Analysis

Table 1 lists the main lines and gives the minimum energy of the in-coming  $\alpha$ -particle needed for them to be created. The variation of yield with energy is in part due to these threshold effects. Below 4 MeV we do not have much data to work with and so extrapolation could be adding to the overall (but unknown) error. This is important to be aware of because the  $\alpha$ -spectrum from uranium is rather soft being concentrated in the 4 MeV to 5 MeV range. Despite this caution however, we empirically find that the  $\alpha$ -induced gamma production rate to the  $\alpha$ -induced neutron production rate is rather insensitive to  $\alpha$ -energy which make our conclusions quite robust.

Note, the 1,275 keV line may be generated as shown as a result of the  $(\alpha, p)$  reaction. However, every  $F(\alpha, n)$  reaction creates a  $^{22}Na$  nucleus which decays with a half-life of about 2.6 years with the emission of the same 1,275 keV line. Thus the intensity of the 1275 keV line in an actual spectrum will be dependent on the age of the  $UF_6$ . The intensity will also be enhanced over the  $(\alpha, p)$  route. Note also that there is a nuisance unresolved reaction line at about 1,280 keV that has a threshold of about 4.7 MeV which could cause potential interference. The 583 keV line

has a potential interference with thorium present in the environment or coming from  $^{232}\text{U}$  if recycled feed has been used.

**Table 1. Principle lines, originating reaction, and energy thresholds.**

Line Energy / keV	Reaction Type	$\alpha$ -energy threshold / keV
110	( $\alpha, \alpha'$ )	133.0
197	( $\alpha, \alpha'$ )	238.6
583	( $\alpha, n$ )	3068.3
891	( $\alpha, n$ )	3440.9
1236	( $\alpha, \alpha'$ )	1629.0 (via 1346 keV level)
1275	( $\alpha, p$ )	0
1528	( $\alpha, n$ )	4212.3

Table 2 summarizes the relevant thick target integrated over angle specific yields calculated in this work for  $\text{UF}_6$ . In principle these numbers should be obtainable with a relative uncertainty of 1-3% at the 68% confidence level. However known inconsistencies in data of this kind lead us to suggest an uncertainty of 20% or more would be more indicative of reality. Important for comparison is the specific yield of the 186 keV line emitted following the decay of  $^{235}\text{U}$ . This is roughly  $45.7 \times 10^3$   $\gamma/\text{sec}/\text{gram}$ .

**Table 2. Specific yields in  $\text{UF}_6$  for the naturally occurring isotopes of uranium. Listed are the total neutron production rates from both ( $\alpha, n$ ) and SF. In the case of the 1275 keV  $\gamma$ -line only the direct ( $\alpha, p$ ) production route is considered.**

Emission	$^{234}\text{U}$ (particle/sec/gram)	$^{235}\text{U}$ (particle/sec/gram)	$^{238}\text{U}$ (particle/sec/gram)
( $\alpha, n$ )	607	0.118	0.0121
(SF, n)	0.00671	$1.1 \times 10^{-5}$	0.0133
110 keV $\gamma$	147	$2.63 \times 10^{-2}$	$2.64 \times 10^{-3}$
197 keV $\gamma$	452	0.0899	$9.75 \times 10^{-3}$
583 keV $\gamma$	109	$1.74 \times 10^{-2}$	$1.67 \times 10^{-3}$
891 keV $\gamma$	89.7	$2.08 \times 10^{-2}$	$2.61 \times 10^{-3}$
1,236 keV $\gamma$	24.0	$3.29 \times 10^{-3}$	$2.86 \times 10^{-4}$
1,275 keV $\gamma$	306	$7.08 \times 10^{-2}$	$8.63 \times 10^{-3}$
1,528 keV $\gamma$	27.1	$5.01 \times 10^{-3}$	$4.95 \times 10^{-4}$
1528 keV $\gamma$	27.1	$5.01 \times 10^{-3}$	$4.95 \times 10^{-4}$

## VI.F. Experimental Results

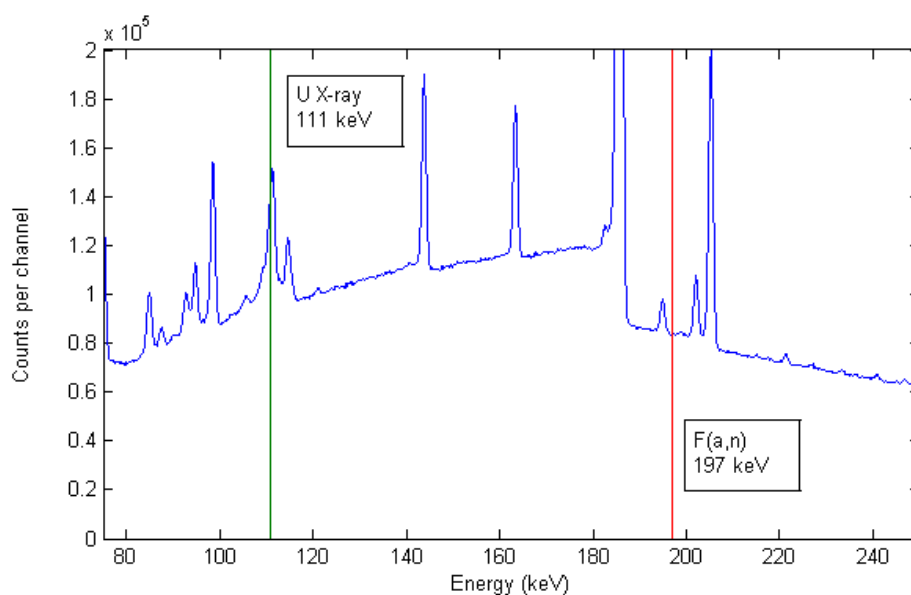
For illustration we present findings from a spectrum collected from a  $\text{UF}_6$  product cylinder. The wall was made of steel approximately 12.8 mm thick. The  $\text{UF}_6$  inside had an enrichment of approximately 4.4 wt% and was derived from natural U feed. The age of the cylinder was approximately 5½ years.

The data was acquired using a high purity Ge detector of the Broad Energy Germanium (BEGe) type with approximate dimensions 60 mm diameter and 30 mm thick. It was fitted with a side shield and the open face viewed bulk material inside the cylinder.

The duration of the data acquisition was 13,598 sec live time, 17,255 sec clock (elapsed) time. The energy range covered approximately 1,377 keV using a conversion gain of 0.1681 keV/chan and a 8,192 channel spectrum. This cuts off any possibility of observing the 1,528 KeV line.

The entire spectrum is displayed in three panels (Figure 1) chosen to cover the experimental energy range in detail suitable for viewing. From inspection of the plots we note that: the 110 keV line is very close to a U X-ray at 111 keV and is not discernible; no peak is apparent at 197 keV to the side of the weak (about 1 % of the 186 keV line strength) line at 195 keV coming from  $^{235}\text{U}$  decay; there is perhaps a weak peak at 583 keV but it is most likely from  $^{228}\text{Th}$ ; the 891 keV is not detected; in the vicinity of 1,236 keV we have a problem with 1,237.22 keV line from  $^{234\text{m}}\text{Pa}$ ; we see the 1,275 keV line clearly, and as discussed above this has two production channels and the intensity is age dependent.

To conclude, even in this spectrum with a long count time and reasonably large area Ge detector, the 1,275 keV is the only  $F(\alpha, \gamma)$  feature observed. Its strength could help verify an operator declaration provided other acceptable knowledge is available (especially the age). The other  $F(\alpha, \gamma)$  lines are concealed by the dominant uranium line spectrum and associated continuum, for instance downscatter of the 1,001 keV line in the  $^{238}\text{U}$  decay series and  $\beta$ -bremsstrahlung.



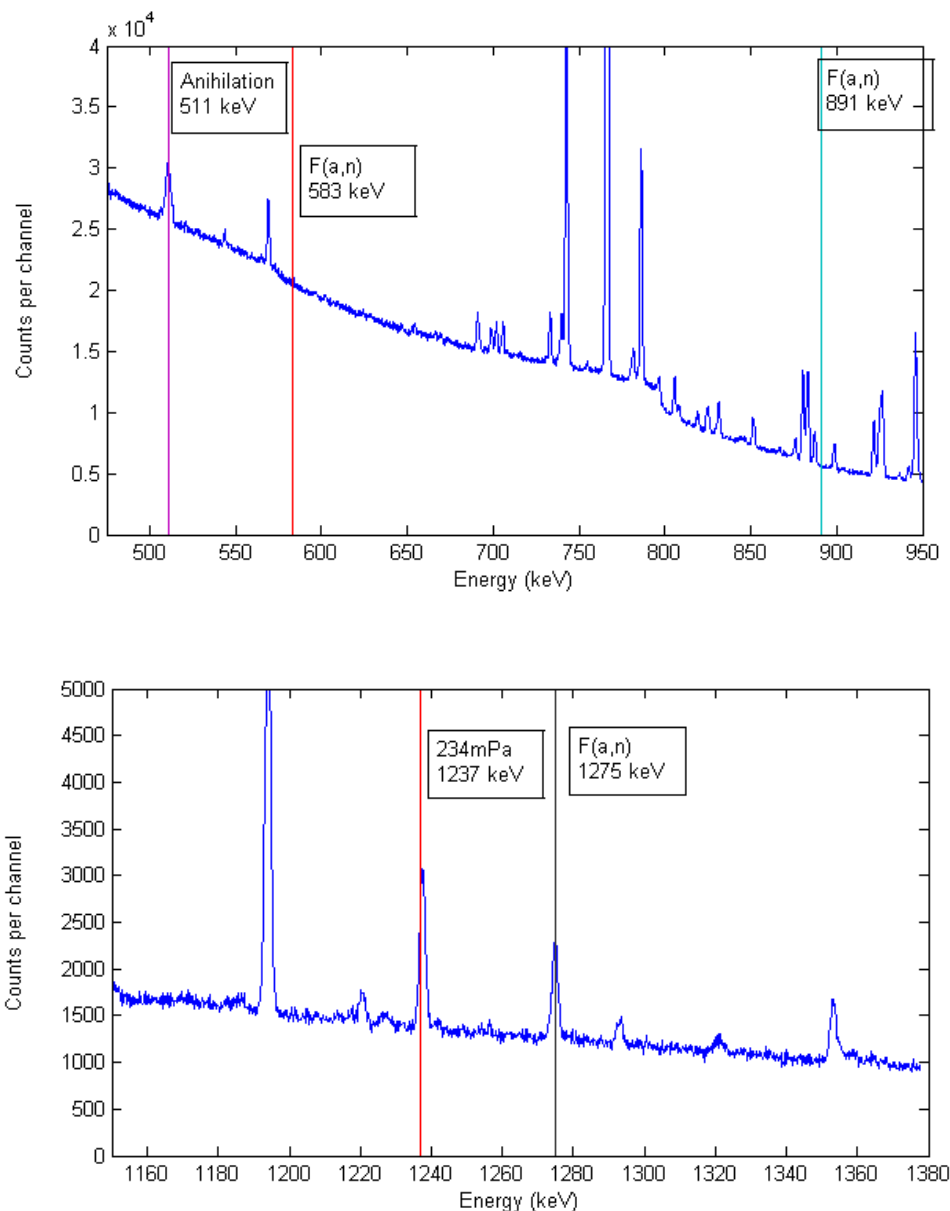


**Figure 1.** A high resolution BEGe gamma-ray spectrum from a cylinder of  $\text{UF}_6$  containing uranium enriched to approximately 4.4 wt% in  $^{235}\text{U}$ . The spectrum was acquired for a period of about 3.8 hrs. With the exception of the 1,275 keV peak, there is no evidence of the  $\alpha$ -particle reaction gamma-lines from fluorine visible above the uranium spectrum.

## VI.G. Discussion

From Table 2 it is clear that the reaction  $\gamma$ -lines are produced and with similar (order of magnitude) strength to the reaction neutrons.

We stop short of providing a detailed and specific analysis across the full dynamic range here mainly because the  $^{234}\text{U}$ : $^{235}\text{U}$  ratio as a function of enrichment is usually considered proprietary. However the following simplistic example will suffice to make the salient point which is general.

Consider product enriched to 5 wt%, towards the upper end of commercial use and consequently in the domain where the  $^{234}\text{U}$  abundance will be highest and give us the best chance of detecting reaction  $\gamma$ -rays. Let us assume the  $^{234}\text{U}$  abundance is 1% of the  $^{235}\text{U}$  content. This is on the high side but not outlandish. The strongest reaction line is at 197 keV. So let us consider that. It is also close to the 186 keV line in energy and so to first order will emerge from a similar amount of  $\text{UF}_6$ , suffer a similar degree of wall attenuation, and be detected with similar full energy peak efficiency. In this contrived example, for every gram of U we have 0.0005 g of  $^{234}\text{U}$ , 0.05 g  $^{235}\text{U}$  and 0.9495 g of  $^{238}\text{U}$ . Using the conversion coefficients in Table 2 we find the following. Total neutron production is about 0.33 n/sec/gram of U. The ratio of the 197 keV  $\gamma$  production to primary neutron product is about 0.72. Thus the gamma source strength and the neutron source strength are of similar magnitude on a per gram basis.

In stark contrast the relative production rate of the 197 keV line to that of the 186 keV line on a per gram of uranium basis is almost exactly four orders of magnitude lower. Thus, in a field measurement designed to quantify the 186 keV line with a few percent precision, the 197 keV line will remain hidden in the statistical noise.  $\text{F}(\alpha, \text{n})$  reaction  $\gamma$ -ray analysis for the purpose of determining the  $^{234}\text{U}$  abundance is therefore clearly not viable for normal safeguards applications. The count time required to obtain a few percent precision would be prohibitive. This technique is, however, a viable option for special circumstances, for instance where the  $^{234}\text{U}$  content of a cylinder is in question and long count times are permissible. It can be a more cost effective and timely alternative to destructive analysis.

It is interesting to ask why, when the reaction gamma production rate is similar to that of the neutron signature why neutron detection provides such a strong signal when the reaction gamma rate does not. It is because 1) neutron detectors can be big, covering a significant fraction of solid angle and with far greater collecting power than a single collimated Ge crystal, 2) the intrinsic efficiency of a neutron detector can also be large, larger than the photo-peak intrinsic efficiency, 3) neutrons are almost unaffected by the container wall where as gamma-ray in this domain are strongly attenuated, 4) neutrons can be collected from the bulk of the  $\text{UF}_6$ , where as gamma-rays emerge only from the skin, 5) finally, the neutron signal may obtain some boost from induced fission.

## VI.H. Future Work

The data base for  $\alpha$ -induced neutron and gamma production is sparse and subject to large experimental uncertainties. Although adequate for this work, in general the uncertainties are much larger than one might expect given the potential of radiometrology and are also much larger than needed to support other technological applications. Therefore attention needs to be directed at improving the values of the basic cross-sections and yield and especially the quantification and reporting of appropriate associated uncertainties.

## VI.I. Conclusions

We have incorporated  $\alpha$ -induced gamma production data for fluorine into a code enabling the specific uranium nuclide thick target production rates in  $\text{UF}_6$  to be computed. We can now calculate yields for a variety of targets and nuclides in a straight forward fashion. We showed



that the  $\gamma/n$  ratio is reasonably flat although subject to scaling uncertainty. Comparison of the reaction gamma yield to the 186 keV line from  $^{235}\text{U}$  indicated that the reaction rates are too weak to be used as an independent and direct check on the  $^{234}\text{U}$  abundance for practical purposes at commercial gas centrifuge enrichment plants. When one factors in the continuum and potential interferences present in realistic spectra the problem is exasperated further. Reprocessed feed containing  $^{232}\text{U}$  makes things even worse in this regard. Our conclusions are in full accord with our initial observations from spectra gathered from cylinders in the field, and a spectrum acquired from 68 wt% enriched material gave no discernible direct reaction gamma line intensity.

## VI.J. References

1. P. Matussek, "Accurate determination of the  $^{235}\text{U}$  isotope abundance by gamma spectrometry," Kerforschungszentrum Karlsruhe Report KfK 3752 (Mai, 1985).
2. K.A. Miller, M.T. Swinhoe, J.B. Marlow, H.O. Menlove, C.D. Rael, T. Iwamoto, T. Tamura and S. Aiuchi, "The uranium cylinder assay system for enrichment plant safeguards," J. Nucl. Mater. Man. XXXIX No. 1(Fall, 2010)21-25.
3. K.A. Miller, H. O. Menlove, M. T. Swinhoe and J. B. Marlow, "The Passive Neutron Enrichment Meter for Uranium Cylinder Assay," ESARDA Bulletin 46(Dec., 2011)115-120.
4. A. M. LaFleur, K. A. Miller, H. O. Menlove, M. T. Swinhoe and J. B. Marlow, "Verification of Small  $\text{UF}_6$  Cylinders Using Neutron Self-Interrogation and Multiplicity Counting," Proc. 52<sup>nd</sup> Annual INMM Meeting, July 2011 Palm Desert, CA, USA.
5. Here you will find information for the nuclear reaction of interest:  
<http://www.nndc.bnl.gov/exfor/exfor00.htm>
6. S. Croft, R. Venkataraman and C.G. Wilkins, "Gamma Ray to Neutron Production Rates for  $\alpha$ -Particle Induced Reactions on Li, Be, B, C and F," Proceedings WM'04, February 29-March 4, 2004 Tucson, Arizona, USA. Waste Management, Energy Security and a Clean Environment. HLW, TRU, LL/ILW, Mixed Hazardous Waste and Environmental Management. © WM Symposia, Inc. Paper WM-4283.
7. S. Croft, "The thick target ( $\alpha,n$ ) yield of fluorine compounds for a broad range of actinides," 19<sup>th</sup> Annual ESARDA (European Safeguards Research and Development Association) Symposium on Safeguards and Nuclear Material Management, Montpellier, France, May 13-15, 1997. ESARDA 28 EUR 17665 EN(1997) 397-404.
8. S. Croft, L. C-A. Bourva and C.G. Wilkins, "The ( $\alpha, n$ ) Production Rate in Plutonium Fluoride," 25<sup>th</sup> Annual Meeting ESARDA (European Safeguards Research and Development Association) Symposium on Safeguards and Nuclear Material Management, Stockholm, Sweden, 13-15 May 2003. EUR 20700 EN (2003) Paper P095. ISBN 92-894-5654-X.
9. J.A. Chapman, S. Smith, A. Lousteau and S. Croft, "Calibration of Passive Neutron Counters Based on an Uncertain Neutron Source Term," Proceedings of the 51<sup>st</sup> Annual Meeting of the Institute of Nuclear Materials Management, July 11-15, 2010, Baltimore, MD, USA. CD ROM.
10. E.R. Norman, K.T. Lesko, T.E. Chupp, P. Schwalbach, and M.A. Faccio, "Gamma-ray production cross sections for alpha-particle induced reactions on  $^{19}\text{F}$  and  $^{23}\text{Na}$ ," Radiation effects 94/1-4(1986)307-310.
11. M.J. Berger, J.S. Coursey, M.A. Zucker and J. Chang, "Stopping-power and range tables for electrons, protons, and helium ions," The National Institute of Standards and Technology (NIST) report NISTIR-4999(2005), Numerical data is available on-line at:  
<http://physics.nist.gov/PhysRefData/Star/Text/ASTAR.html>
12. P M J Chard and S Croft, "A database of  $^{240}\text{Pu}_{\text{effective}}$  and  $^{235}\text{U}_{\text{effective}}$  coefficients for various fertile and fissile isotopes," 19<sup>th</sup> Annual ESARDA (European Safeguards Research and Development Association) Symposium on Safeguards and Nuclear Material Management, Montpellier, France, May 13-15, 1997. ESARDA 28 EUR 17665 EN(1997) 389-396.

## VII. ELECTROMAGNETIC AND ACOUSTIC NDE TECHNIQUES TO AID IN UF<sub>6</sub> ENRICHMENT VERIFICATION

*Jacob Benz, Christopher Orton, Ben McDonald, Mark Jones, Pradeep Ramuhalli  
Pacific Northwest National Laboratory*

### VII.A. Introduction

Non-destructive evaluation (NDE) techniques are complementary to non-destructive assay (NDA) and can be used to increase the confidence and accuracy in enrichment measurements of UF<sub>6</sub>. This paper will focus on electromagnetic and acoustic techniques, and how they can potentially be utilized to address issues of concern for NDA affecting the quality and accuracy of enrichment measurements.

In regards to UF<sub>6</sub> cylinder enrichment verification, there are four main areas where electromagnetic and acoustic techniques may prove useful. The first is wall thickness, which has a large effect on the accuracy of gamma methods to determine enrichment. According to Ref. [1], wall thickness of a 30B cylinder has been shown to vary between 12.5mm and 13.8 mm and a variation of 0.5mm in wall thickness without correction leads to a minimum error of 5% in the enrichment calculation of the UF<sub>6</sub> based on the assay of the 186 keV peak. The IAEA currently uses an ultrasonic gauge to determine the wall thickness at NDA measurement locations to minimize this error.

The second area where NDE methods may help is correcting for filling profile variations within a UF<sub>6</sub> cylinder, which can have a considerable effect on the systematic uncertainty of neutron-based measurements to determine enrichment. Due to the physical properties of UF<sub>6</sub>, there may be two distinct profiles of how the material is arranged within the cylinder. If it has been filled by introducing the material as a liquid, or if the full cylinder has been exposed to hot environmental conditions, or experienced mechanical shocks from transportation then the majority of the material will collect at the bottom, likely leaving a small ring of condensed material covering the top portion of the cylinder wall. If the cylinder is filled through desublimation and environmentally controlled, then there will be an even ring of UF<sub>6</sub> material over the entire cylinder wall. Figure 1 (of Ref. [1]) shows a visual representation of the two filling profiles. Additionally, there may be a whole suite of combinations of the two profiles due to handling and storage conditions. The filling profile within the cylinder will affect the multiplication of neutrons within the UF<sub>6</sub> volume. Uncertainty in the multiplication factor would affect measurements on 30B product cylinders due to the preferentially enriched levels of U-235 (and U-234). [Ref. 7]

The third area of potential usefulness is locating hidden objects, material or gaps within the cylinder.

The final area where NDE techniques may prove useful will be for unique identification of cylinders. This is a very important tool to maintain continuity of knowledge over the UF<sub>6</sub> in the cylinders, and can be applicable to an unattended measurement station.

## VII.B. Potential Application of Acoustic and Electromagnetic Techniques to Assist with NDA Measurements of UF<sub>6</sub>

Currently, high energy linacs are required to penetrate the high density UF<sub>6</sub> solid to detect density changes of material inside cylinders, which does not lend itself easily for use by inspectors, or for unattended measurements. Acoustic measurement techniques provide a simple alternative method to potentially interrogate the entire contents of a UF<sub>6</sub> cylinder. Varying the wavelength of an acoustic pulse introduced at the cylinder wall will allow the signal to penetrate deeper into the cylinder. This is the concept behind an ultrasonic gauge currently used by the IAEA to measure cylinder wall thickness. By increasing the wavelength, the acoustic wave will travel beyond the wall and begin to interrogate the interior volume of the cylinder. In this manner it would be possible to determine 1) if there are any hidden objects inside the cylinder and 2) what the filling profile is. Both of these can be determined by introducing an ultrasonic wave into the cylinder, and detecting the reflection signature from the incident pulse wave. This method is used commonly in a variety of other industries to detect contraband or defects within containerized objects (Refs. [2] and [3]). However, the percentage of container interior volume that is interrogated can be negatively impacted by the presence of large voids in the UF<sub>6</sub> solid. Another potential benefit of these methods, if the cylinder remains under controlled conditions, and the filling profile stays consistent, is that it might also be possible to determine if any UF<sub>6</sub> has been introduced or removed by measuring the thickness of the ring (for example with filling by desublimation). When filled as a liquid, the height of the bottom layer can be measured to ensure material has not been removed.

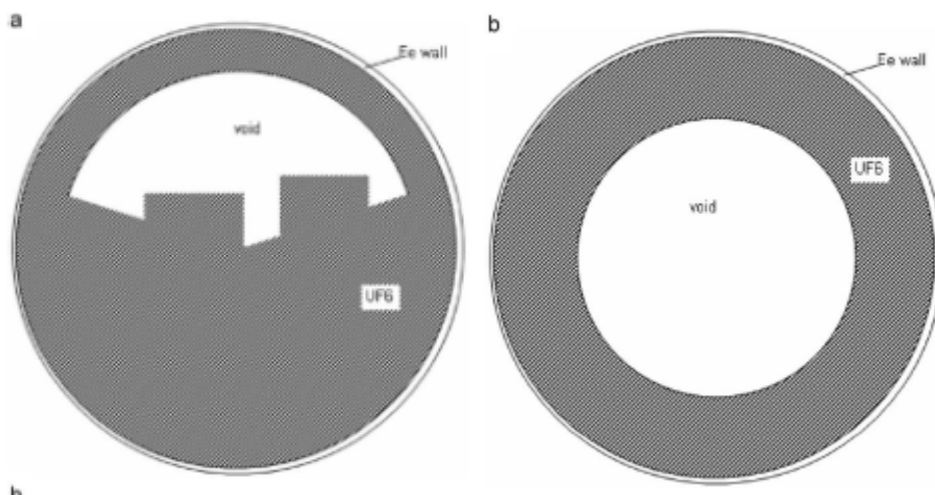


**Figure 1. Filling Profile a) after heating above 80°C and b) after desublimation (Ref. [1]).**

Ultrasonic measurements may also be able to address the issue of unique cylinder identification. The Ultrasonic Intrinsic Tag (UIT) Ref. [4] was first developed in 1989 for use under START to uniquely identify strategic mobile missile components, typically first stage rocket motors. In the same manner described above, a high frequency ultrasonic pulse was introduced into the material under interrogation, and the backscatter profile from the ultrasonic wave due to the unique grain structure of the material itself was recorded as the intrinsic identification for that object. The initial prototypes were fabricated to evaluate polymer-based, fiber reinforced composite structures (first stage rocket motors), and the depth of the measurement was on the order of 3 to

5 mm. Improvements to the technology now allow measurement depths as shallow as 1 mm for unique identification of thin metallic alloy shells. In all cases, the subsurface signature generation and extraction method prevents the signature from changing due to normal operations, or from tamper to purposefully subvert the signature. Additionally the material and depth of measurement are flexible by changing the frequency of the ultrasonic wave. The same process could be applied to UF<sub>6</sub> cylinders to uniquely identify each cylinder throughout a given process or set of processes.

There are several low-frequency electromagnetic measurement techniques that can potentially be used to uniquely identify cylinders. The PNNL EM Coil (Ref. [5]) was also developed under the auspices of a U.S. – Russia bilateral arms control treaty. The EM Coil is a large-scale eddy current measurement system in which an encircling coil completely surrounds the metallic object under interrogation. The eddy currents induced in the object creates a secondary field which produces a coil impedance signature based on the properties of the entire object and everything contained within. The excitation field is swept through multiple frequencies in order to create the signature. This method has been shown to produce distinct signatures for different materials inside the same type of container. Weld points are a particularly useful measurement location due to the unique and random manner in which the welds are produced. It is anticipated that an EM Coil constructed to measure the weld locations between the main cylinder body and skirt protecting the end caps may provide a unique frequency-dependent signature for cylinder identification.

Small-scale eddy current measurements may also be useful for unique cylinder identification and tamper detection (Ref. [6]). These measurements are based on the same electromagnetic phenomenon (mutual induction) as the EM Coil. However, in this configuration a small-diameter coil is wound around a wand which can be passed across the surface under interrogation rather than surrounding the object. An array of coils mounted on a flexible substrate could be used to inspect the cylinder surface in a rapid or automated manner. Therefore the small-scale eddy currents are not being utilized to interrogate the entire container, but only the surface under examination. Unique identification can be performed by measuring the frequency-dependent electrical impedance of the coil as it passes over the weld locations. The concept of tamper indication is also provided in Ref. [6] where Sandia National Laboratories developed an eddy current scanner to detect tampering of 3013 containers. It is anticipated that small-scale eddy current measurements can detect very small tampered and repaired locations, even those not visible to the naked eye, and could be adapted to detect unauthorized intrusion into UF<sub>6</sub> cylinders.

### **VII.C. Conclusions**

Acoustic and electromagnetic NDE techniques are complementary to NDA measurements, and may improve the accuracy and continuity of knowledge of UF<sub>6</sub> measurements of interest to the IAEA. Acoustic and ultrasonic measurements are routinely performed in other industries to address similar issues, such as wall thickness determination and interrogation of pipes and containers to determine fill level and the presence/absence of hidden objects.

As a final comment, it may be possible to incorporate these methods into an unattended measurement station. According to Ref. [1], wall thickness measurements are not possible for unattended measurement systems because contact is required to make the measurement. However, a pressure plate could be incorporated onto the base of the cylinder stand which is

depressed when a cylinder is placed on it. Once depressed, a signal could trigger hydraulic arms containing the acoustic/EM equipment which would surround the cylinder and ensure good contact and consistent measurements.

#### VII.D. References

1. R. Berndt, E. Franke, P. Mortreau, “ $^{235}\text{U}$  enrichment or  $\text{UF}_6$  mass determination on  $\text{UF}_6$  cylinders with non-destructive analysis methods,” Nuclear Instruments and Methods in Physics Research A, 612, 2010, 309-319.
2. T.H. Gan, D.A. Hutchins, D.R. Billson, F.C. Wong, “Ultrasonic Tomographic Imaging of an Encased, Highly Attenuating Solid Medium,” Research in Nondestructive Evaluation, 13, 2001, 131-152.
3. P. Shull, H. Felix Wu, A. Diaz, “Through container measurement of acoustic signatures for classification/discrimination of liquid explosives and precursor threat liquids,” Nondestructive Characterization for Composite Materials, Aerospace Engineering, Civil Infrastructure, and Homeland Security, Conference Proceedings Vol. 6934, 2008.
4. M. S. Good, B. E. Simpkins, L. J. Kiriara, J. R. Skorpik, J. A. Willett, “Ultrasonic Intrinsic Tagging for Nuclear Disarmament: A Proof-of-Concept Test”, PNNL-14462, Pacific Northwest National Laboratory, Richland, Washington, 2003, [http://www.pnl.gov/main/publications/external/technical\\_reports/PNNL-14462.pdf](http://www.pnl.gov/main/publications/external/technical_reports/PNNL-14462.pdf) (accessed March 2012).
5. A.M. Jones, K.J. Bunch, and P.M. Aker, to be published 2012, “Simulation and Experimental Validation of Electromagnetic Signatures for Monitoring of Nuclear Material Storage Containers,” Journal of Nuclear Materials Management.
6. K. Tolk, G. Stoker, “Eddy Current Testing of Welded Stainless Steel Storage Containers to Verify Integrity and Identity,” SAND99-1829C.
7. K.A. Miller, H.O. Menlove, M.T. Swinhoe, J.B. Marlow, “A New Technique for Uranium Cylinder Assay Using Passive Neutron Self-Interrogation”, IAEA-CN-184/131.